Title: A genome-wide CRISPR/Cas9 screen identifies genes that regulate the cellular uptake of α-synuclein fibrils by modulating heparan sulfate proteoglycans

Authors:

Vanderperre, B.[1,2,4#], Muraleedharan, A.[1,2], Dorion, M.-F.[3], Larroquette, F.[4], Del Cid Pellitero, E.[4], Rajakulendran, N.[5], Chen, C. X.-Q.[3], Larivière, R.[4], Michaud-Tardif, C.[4], Chidiac, R.[5], Lipuma, D.[1,2], MacLeod, G.[5], Thomas, R.[3,4], Wang, Z.[6], Reintsch, W.E.[3], Luo, W.[3], Shlaifer, I.[3], Fuming, Z.[7], Xia, K.[7], Yan. L[7], Steinhart, Z.[5], Linhardt, R.J.[7], Trempe, J.-F.[8], Liu, J.[6], Durcan, T.M.[3], Angers, S.[5], Fon, E.A.[4,#]

Affiliations:

[1]Département des Sciences biologiques, Université du Québec à Montréal, Montréal, QC, Canada.
[2]Centre d'Excellence de Recherche sur les Maladies Orphelines – Fondation Courtois (CERMO-FC).
[3]The Neuro's Early Drug Discovery Unit (EDDU), Department of Neurology and Neurosurgery, Montreal Neurological Institute-Hospital, McGill University, Montreal, QC, Canada.
[4]McGill Parkinson Program, Department of Neurology and Neurosurgery, Montreal Neurological Institute and Hospital, McGill University, Montréal, QC, Canada.
[5]Leslie Dan Faculty of Pharmacy, University of Toronto, Toronto, ON, Canada.
[6]Division of Chemical Biology & Medicinal Chemistry, Eshelman School of Pharmacy, University of North Carolina, Unites States of America.
[7]Department of Chemistry and Chemical Biology, Rensselaer Polytechnic Institute, Troy, NY, Unites States of America.
[8]Department of Pharmacology & Therapeutics and Centre de Recherche en Biologie Structurale, McGill University, Montréal, QC H3G 1Y6, Canada.
[#] corresponding authors: vanderperre.benoit@uqam.ca; ted.fon@mcgill.ca

Keywords: alpha synuclein, CRISPR/Cas9, genome-wide screen, Parkinson's disease, heparan sulfate proteoglycans, preformed fibrils, protein aggregates

ABSTRACT

Synucleinopathies are characterized by the accumulation and propagation of α-synuclein (α-syn) aggregates throughout the brain, leading to neuronal dysfunction and death. Understanding how these aggregates propagate from cell to cell in a prion-like fashion thus holds great therapeutic promises. Here, we focused on understanding the cellular processes involved in the entry and accumulation of pathological α-syn aggregates. We used an unbiased FACS-based genome-wide CRISPR/Cas9 knockout (KO) screening to identify genes that regulate the accumulation of α-syn preformed fibrils (PFFs) in cells. We identified key genes and pathways specifically implicated in α-syn PFFs intracellular accumulation, including heparan sulfate proteoglycans (HSPG) biosynthesis and Golgi trafficking. We show that all confirmed hits affect heparan sulfate (HS), a post-translational modification known to act as a receptor for proteinaceous aggregates including of α-syn and tau. Intriguingly, KO of *SLC39A9* and *C3orf58* genes, encoding respectively a Golgi-localized exporter of Zn^{2+}, and the Golgi-localized putative kinase DIPK2A, specifically impaired the uptake of α-syn PFFs uptake but not of tau oligomers, by preventing the binding of PFFs to the cell surface. Mass spectrometry-based analysis of HS chains indicated major defects in HS maturation in *SLC39A9* and *C3orf58* KO cells, explaining the cell surface binding deficit. Our findings now clearly establish these two genes as HSPG-modulating factors. Interestingly, *C3orf58* KO human iPSC-derived microglia exhibited a strong reduction in their ability to internalize α-syn PFFs. Altogether, our data establish HSPGs as major receptors for α-syn PFFs binding on the cell surface and identifies new players in α-syn PFFs cell surface binding and uptake.

INTRODUCTION

Synucleinopathies are a class of neurodegenerative disorders that include Parkinson's disease (PD), Dementia with Lewy Bodies (DLB), and Multiple System Atrophy (MSA)[1]. The molecular hallmark of these neurodegenerative diseases is the presence in the brain of aggregates composed mainly of the protein α-synuclein (α-syn)[2]. In these diseases, α-syn misfolds and aggregates in a prion-like amyloidogenic cascade culminating, in PD, in the formation of higher order aggregates termed Lewy bodies (LBs) and Lewy neurites. Similar to other proteinopathies, evidence suggests that cell-to-cell transmission of α-syn aggregates underlies disease progression[3,4]. It was first exemplified by the appearance of LBs in initially healthy grafted tissue following transplantation in the brain of a PD patient[5]. Later on, in vitro experiments and the use of animal models have confirmed that α-syn preformed fibrils (PFFs) made of recombinant α-syn can reach the intracellular compartment in a wide variety of cell types[6–9]. This is followed by self-templated aggregation of native cytosolic α-syn, and transmission of newly formed aggregates to neighboring cells by a variety of proposed mechanisms, including the secretion of exosomes[10], tunneling nanotubes[11,12], trans-synaptic spread[13], or misfolding-associated protein secretion[14].

The molecular mechanisms underlying these events are poorly understood. This is especially the case for the entry of extracellular aggregates in recipient cells, where several endocytic pathways (clathrin-dependent[15,16] and independent[17] endocytosis, macropinocytosis[18,19]) and surface receptors (LAG3[20], heparan sulfate proteoglycans (HSPGs)[16,18], neurexin 1β[21]) have been identified, likely because of the variety of cellular models or libraries used in overexpression screens. Because spreading could potentially be driven by several cell types within the brain[22–24], it is important to unravel mechanisms and molecular players that underly this cell-to-cell transmission across cell types, but that are also sufficiently specific to α-syn aggregates uptake to prevent advert effects of possible therapies.

In this regard, HSPGs are a very promising class of receptors, having been shown to mediate α-syn PFF uptake in several neural cell types including mouse primary neurons[16,18] and neuroblastoma, oligodendrocyte-, astrocyte- and to a lesser extent microglia-like cell lines[25]. HSPGs are cell surface and extracellular matrix (ECM) proteins that are post-translationally modified with heparan sulfate (HS) chains composed of disaccharide units[26]. HSPG biosynthesis starts in the endoplasmic reticulum (ER) and continues in the Golgi apparatus where the exostosin complex (composed of EXT1 and/or EXT2) catalyzes the elongation of the disaccharide chain[26]. Modification of the HS chain then occurs also in the Golgi, mainly by sulfation (which adds negative charges) at various positions of disaccharide units by several sulfotransferases, using PAPS (3′-phosphoadenosine-5′-phosphosulfate) as a sulfate donor[27]. Depending on the core protein that bears the HS moieties, plasma-membrane HSPGs fall mainly in two classes: the membrane integral syndecans (SDC) or glycosylphosphatidylinositol-anchored glypicans (GPC)[26]. Once they reach the cell surface, HSPGs expose their negatively charged HS chains to serve as membrane receptors and co-receptors for a wide range of positively charged cargoes[26,28]. Recently, it was shown that knock-out (KO) of the SLC35B2 transporter, responsible for PAPS import into the Golgi and sulfation of HS, drastically reduces the uptake of α-syn PFFs by HEK293T cells and mouse primary neurons[16]. This study uncovered a general mechanism of HSPG-dependent cell surface binding of positively charged cargoes is necessary for uptake of α-syn PFFs, even if several endocytic mechanisms may substitute for one another (e.g. clathrin-mediated endocytosis[16], macropinocytosis[18]) downstream of HSPG binding. Therefore, identifying α-syn PFFs-specific modulators of HSPG-dependent cell-surface

binding could prove very useful to develop therapies aiming at reducing the intercellular spread of α-syn aggregates, while preventing adverse effects that global HSPG impairment could cause.

In the present study, we aimed at identifying cellular factors affecting the uptake of α-syn PFFs using an unbiased genome-wide CRISPR/Cas9 KO screen in human cells. Our screen confirmed that HSPGs are major receptors for α-syn PFFs, with several genes identified regulating HSPG expression, and uncovered new genes, the silencing of which strongly and specifically inhibit α-syn PFF uptake. More specifically, we found that loss of C3orf58 (also termed DIPK2A), a putative kinase in the Golgi, or SLC39A9, a Zn^{2+} exporter in the Golgi membrane, results in marked perturbations in HS expression and composition, which was associated with a large reduction in PFF uptake secondary to decreased PFF binding to the cell surface. We also show that *C3orf58* is necessary for PFF uptake in human iPSC-derived microglia. Overall, our study provides an unprecedented, pathway-level view of α-syn PFFs uptake mechanisms that will help in the design of future therapeutic strategies.

RESULTS

Genome-wide CRISPR screening identifies genetic modifiers of α-syn PFF accumulation

To identify key genes involved in α-syn PFF accumulation in human cells, we performed a FACS-based, pooled genome-wide CRISPR/Cas9 knock-out screen in a transformed Retina Pigmented Epithelial cell line (RPE-1) **(Figure 1A)**. RPE-1 cells were infected with the lentiviral Toronto Knock-Out Library (v3)[29] at low multiplicity of infection (MOI), targeting >18,000 genes with >71,000 individual sgRNAs (app. 4 sgRNAs per gene), including non-targeting control (LacZ, EGFP, Luciferase). Transduced cells were selected with puromycin and amplified, yielding a population of genetically perturbed cells where the vast majority of cells received only one sgRNA. We then performed a 24-hour treatment with fluorescently labeled α-syn PFFs (see **Supplementary Figure 1A, B** for transmission electron microscopy analysis of PFFs). Cells with the 15 % lowest and 15 % highest PFF fluorescence were then isolated by FACS. Next generation sequencing was used to identify the sgRNAs present in each population, and sgRNAs/target genes enrichment analysis between the two populations was performed using the MAGeCK algorithm[30] **(Figure 1B, Tables S1, S2, S3)**. Genes enriched in the "Low PFF" population represent putative facilitators of α-syn PFFs accumulation, because disrupting them results in lower PFF amount per cell. Conversely, genes enriched in the "High PFF" population are putative inhibitors of PFF accumulation. Gene ontology analysis **(Figure 1C)** indicated that genetic facilitators of PFF accumulation were mainly associated with Golgi vesicle trafficking (*COPB1*, *COPG1*, *TMED10*), heparan sulfate biosynthesis (*EXT1*, *NDST1*, *SLC10A7*[31], *TM9SF2*, *SLC39A9*), and to a lesser extent phagosome acidification (several v-ATPase subunits). Other well-ranked genes included the cell cycle regulators *TP53* and *CDKN1A* as well as a poorly characterized gene, *C3orf58*. On the other hand, inhibitors of PFF accumulation were, to our surprise mostly related to metabolic processes needed for cell growth and cell cycle such as nucleic acid metabolism. Exceptions were the *MOSPD2* and *STARD3* genes, which encode two interacting proteins that regulate cholesterol transfer from endoplasmic reticulum to endosomes[32], and *VPS35*, which regulates endosomal trafficking and in which mutations cause familial forms of PD[33]. Explaining the identification of genes related to cell cycle/growth, several lines of evidence indicated a clear link between cell size and PFF accumulation. This is described in detail in **Supplementary Figure 2** and prompted us to design a validation strategy that takes into account this cell size bias at play in our screen.

Validation of hits by high-content microscopy

To identify genes that modulate α-syn PFF accumulation independently from effects on cell size, we normalized PFF content to cell size using high-content microscopy **(Figure 2)**. We used RPE-1 cells stably expressing Cas9 and EGFP and transfected them with synthetic sgRNAs against a selection of putative hits (**Figure 2A**; for hits selection criteria, see **Supplementary Figure 3A**). Two sgRNAs per gene were used, one from the tKOv3 library, and one custom sgRNA. Additionally, control sgRNAs targeting the *AAVS1* locus were used to induce double-strand breaks formation similar to those induced by sgRNAs targeting the selected hits. Three days post-transfection, a time at which more than 80 % of cells were successfully gene-edited, as verified using an *EGFP*-targeting sgRNA **(Supplementary Figure 3B)**, we performed a 24 h accumulation assay with fluorescent α-syn PFF. Using high-content microscopic analysis, we quantified the α-syn PFF fluorescent signal normalized to the area of each cell, using an EGFP mask **(Figure 2B)**. Consistent with the possible enrichment of fast-cycling cells in the "Low PFF" population from the screen, knocking-out the tumor suppressors *CDKN1A*, *TP53* and *DYRK1A* significantly

reduced cell size but did not decrease the normalized PFF accumulation. Conversely, knock-out of known oncogenes or genes that mediate G2/M cell cycle transitions (*CDK1, GLN3, KIF11, KIF23, PSMD12/13*) increased cell size at least for one of the two sgRNAs without modifying normalized PFF content, explaining their enrichment in the "High PFF" population of the screen. Importantly, normalization of α-syn PFF content to cell size allowed us to validate 7 facilitators (*C3orf58, COPB1, COPG1, EXT1, NDST1, SLC39A9* and *TM9SF2*) and one inhibitor (the PD-related gene *VPS35*) of α-syn PFF accumulation **(Figure 2B, Supplementary Figure 3C)**. *VPS35* deficiency was previously reported to induce an increase in uptake of amyloid-beta (Aβ) aggregates through an unknown mechanism[34], and it thus appears that *VPS35* could play a broad role in mediating the cellular uptake of various species of protein aggregates. The *EXT1* and *NDST1* genes encode two key biosynthetic enzymes in the biogenesis of heparan sulfate (HS), a post-translational modification that is known to mediate the cellular attachment and entry of α-syn fibrils, as well as FTD-associated tau oligomers[18,35]. In addition, *COPB1* and *COPG1*, encoding two coatamer subunits that mediate retrograde vesicular trafficking in the Golgi apparatus, were previously identified in a screen for cellular entry of *Chlamydia trachomatis* by indirectly impacting HS biogenesis[36]. *TM9SF2* may function in a similar fashion, since TM9SF family proteins have a consensus KxD/E motif (KVD in *TM9SF2*) at the C terminus, which interacts with the *COPI* coatomer[37]. It was previously shown that *TM9SF2* knock-out reduces HS surface expression by affecting proper localization and stability of NDST1[38]. Similarly, knock-out of *SLC39A9*, encoding a Zn^{2+} exporter in the Golgi membrane, results in a small decrease in HS surface expression, possibly explaining its identification as an important factor in Chikungunya virus infection[38]. The molecular and cellular function of C3orf58 (also known as DIPK2A or DIA-1) is unclear. This Golgi localized protein was reported to positively regulate autophagosome-lysosome fusion[39], to act as an insulin-like growth factor receptor 1 ligand[40], to colocalize with β-COP proteins suggesting a role in the secretory apparatus[41]. It might also be a key player in Zika virus infection of neural stem cells through an undefined mechanism[42], which remains to be confirmed.

Cargo specificity of validated hits

We next sought to determine whether the effects of the 8 validated hits were specific for α-syn PFF accumulation or also affected other cargoes. Thus, we tested their ability to also perturb the accumulation of dextran (bulk endocytosis), EGF and transferrin (both receptor mediated endocytosis) as well as tau oligomers (HS-dependent macropinocytosis[18])**(Figure 3, Supplementary Figure 4A)**. Among the seven facilitators of α-syn PFF accumulation, none of the gene KOs decreased dextran, EGF or transferrin accumulation, nor did the silencing of *VPS35* increase the accumulation of these cargoes **(Figure 3A-C)**. On the other hand, consistent with their dependency on HS for internalization, Tau oligomers **(Figure 3D)** accumulated significantly less in *EXT1* or *NDST1* silenced cells, and almost significantly for *TM9SF2*. This confirms previous findings that α-syn PFFs and Tau oligomers accumulate intracellularly via a partially overlapping HS-dependent mechanism[18,35]. This is further illustrated in a competition assay, where co-treatment of RPE-1 cells with Tau oligomers and α-syn PFFs decreased the accumulation of both types of aggregates relative to separate treatments **(Supplementary Figure 4B)**. Similar to its effect on α-syn PFFs (**Figure 3E**) and amyloid-β oligomers[34], silencing of *VPS35* increased the accumulation of Tau oligomers **(Figure 3D)**. Together, these data suggest that the genes identified through our screen specifically modulate the accumulation of proteinaceous aggregates. Two of these (*C3orf58* and *SLC39A9*) were specific for α-syn PFFs.

HS mediate most of α-syn PFF binding at the cell surface

Membrane-bound HS can serve as a primary receptor for certain ligands before endocytosis via a secondary, generally more specific receptor, but it has also been shown to be endocytosed together with its ligand following binding at the cell surface[43]. Of the 8 hits identified in our screen, 6 have been previously linked with defects in HS expression. The EXT1 enzyme catalyzes the elongation of the disaccharide chain (GlcN-GlcNAc), while NDST1 is crucial for N-deacetylation/N-sulfation of GlcNAc residues, thereby regulating the binding of various ligands depending on the extent of sulfation and sulfation pattern of the HS chain. *COPB1* and *COPG1* have been shown to indirectly affect HS surface presentation[36], but because these are core essential genes[44], we did not investigate them further. *SLC39A9* and *TM9SF2* have also been suggested to indirectly affect HS surface expression[38]. In addition, the *SLC35B2* gene, which encodes a PAPS importer in the Golgi that is necessary for HS sulfation, was also well scored in the screen **(Table S1)**, consistent with a previous report identifying it as a key regulator of PFF uptake[16]. Simultaneous perturbation of both *SLC35B2* and its functionally redundant homolog *SLC35B3* in RPE-1 cells significantly reduced PFF accumulation **(Supplementary Figure 5)**. However, the role of *C3orf58* and *VPS35* in HS biology has not been investigated previously.

To further test whether HS are major receptors for α-syn PFF in RPE-1 cells, we first sought to determine if the binding of α-syn PFF to the cell surface was HSPG-dependent. We incubated live cells with labeled PFF on ice to prevent endocytosis and monitored PFF binding at the cell surface by fluorescence microscopy. As expected, pre-treatment with either heparinases (to strip-off HS from the cell surface) or sodium chlorate (to inhibit HS sulfation) strongly reduced binding of α-syn PFF to the cell surface **(Figure 4A, B)**. We also monitored surface HS expression in these intact cells by immunofluorescence using a commonly used antibody against the 10e4 epitope (N-sulfated HS, full epitope unknown[45]). The signal was markedly reduced by heparinases treatment, confirming the specificity of the antibody towards HS. However, despite the strong inhibition of PFF binding to the cell surface following sodium chlorate treatment, 10e4 epitope signal was nearly unaffected, showing that this antibody does not fully capture the complexity of HS chain architecture and modifications. In other words, the 10e4 signal is conserved even in conditions where HS sulfation is inhibited to a degree that functionally interferes with PFF binding. At higher magnification, PFF signal appeared as puncta, >90% of which fully or partially overlapped with HS puncta. However, the remaining PFF signal was less readily colocalized with HS (app. 62% colocalized puncta) upon sodium chlorate treatment, confirming that sulfation of HS plays a key role in PFF binding to HS (**Figure 4C**) as previously reported[25,35]. Together, our data confirms that HS are a major receptor of α-syn PFF, including in RPE-1 cells.

Genes identified in our screen regulate HS homeostasis

Having confirmed that HS are key in mediating PFF binding in RPE-1 cells, we sought to evaluate a possible effect on HS expression of some identified hits not directly implicated in HS biosynthesis (*C3orf58, SLC39A9, TM9SF2, VPS35*). To do so, we generated monoclonal CRISPR-edited cells for these four genes (**Supplementary Figure 6**) as well as rescue lines re-expressing the WT version of the respective proteins (except for TM9SF2). We quantified HS signal with the 10e4 antibody in fixed cells, before or after permeabilization, to quantify cell-surface and total HS respectively **(Supplementary Figure 7A, B)**. In agreement with a previous report[38], *SLC39A9* and *TM9SF2* deficient cells exhibited strongly decreased N-sulfated HS signals, while *VPS35* heterozygous cells (homozygous VPS35 KOs were lethal) had increased levels of HS in permeabilized conditions, compatible with its effect on the uptake of α-syn, tau and Aβ proteinaceous aggregates. These effects could be rescued by reintroducing active forms of the proteins (only in permeabilized conditions for VPS35). *C3orf58* had surprising effects on N-

sulfated HS signal. 10e4 signal was not affected by loss of *C3orf58*, but its over-expression in the rescue line resulted in decreased signals **(Supplementary Figure 7A, B)**. As stated earlier, investigation of a single epitope in the complex HS molecules is insufficient to conclude on the expression and modification of HS. Nevertheless, our results clearly establish that manipulation of expression of all four genes perturbed N-sulfated HS signals to varying degrees, suggesting that they might all act on PFF accumulation by modifying a major receptor for α-syn PFFs, HS.

SLC39A9-mediated Zn^{2+} transport, but not C3orf58 kinase activity, is necessary for α-syn-PFF accumulation

Because *C3orf58* and *SLC39A9* deficiency specifically reduced the accumulation of α-syn PFF but not that of other cargoes, including Tau oligomers, we decided to study more in detail the mode of action of these two genes. SLC39A9 (also known as Zip9) is a Zn^{2+} transporter that was previously proposed to export Zn^{2+} from the Golgi lumen to the cytosol[46,47]. C3orf58 (also termed DIPK2A, Dia1 or HASF) is a predicted transmembrane protein, and member of the FAM69 family of secreted kinases[48] even though its kinase activity has not been confirmed to date. Using stable and constitutive lentivirus-mediated expression of HA-tagged wild-type (WT) SLC39A9 or C3orf58 constructs, we generated rescue lines. C3orf58 possesses a putative transmembrane domain in its N-terminal part **(Figure 5A)**, which was consistent with its insolubility in a sodium carbonate extraction assay **(Supplementary Figure 8A)**. Both proteins were localized to the Golgi apparatus **(Supplementary Figure 8B)**. In order to test the importance of Zn^{2+} transport and putative kinase activity in mediating the effects of respectively SLC39A9 and C3orf58 on α-syn PFF accumulation, we generated mutant constructs by altering residues predicted to disrupt these respective functions. To do so, we used AlphaFold for homology-based 3D structural modeling to identify key residues for the specific predicted activities of both proteins. The D159 and H185 residues of SLC39A9 are predicted to coordinate the Zn^{2+} ion as it reaches the exit of the channel and mutating these two amino acids should thus abolish transport activity of SLC39A9 **(Figure 5B)**. Key residues in the putative active site of C3orf58's kinase domain were also identified: D306 and K198 are predicted to be implicated in ATP-Mg^{2+} binding, while A287 is predicted as the catalytic base that removes a proton from the nucleophilic group **(Figure 5C)**. We generated the SLC39A9 D159A and H185R constructs as well as a K198A-D287N-D306N mutant (3MUT) version of C3orf58 and used these to rescue *SLC39A9* and *C3orf58* KO cells. Following 24 h of treatment with fluorescent α-syn PFFs, PFF accumulation could be rescued to the levels of WT cells upon re-expression of the WT proteins **(Figure 5D)**. Putative kinase-dead (3MUT) C3orf58 also rescued PFF accumulation almost to WT levels, but less efficiently than its WT counterpart. This mutant was correctly localized to the Golgi **(Supplementary Figure 8B)**, so the difference might rather be explained by slightly lower expression levels and/or modified glycosylation (**Supplementary Figure 8C,** two of the 3 mutations add asparagines as potential N-glycosylation sites). This suggests that if C3orf58 does have a kinase activity, it does not play a major role in its ability to facilitate PFF accumulation. Cells expressing SLC39A9 D159A or H185R mutants were unable to rescue PFF accumulation **(Figure 5D)**. This is consistent with the inability of these two mutants to rescue the accumulation of Zn^{2+} in the Golgi apparatus observed in *SLC39A9* KO cells, in contrast to the WT rescue line **(Supplementary Figure 9)**. These results suggest that Zn^{2+} homeostasis in the Golgi is important for PFF accumulation. Note that in *C3orf58* KO, *TM9SF2* KO and *VPS35* heterozygous monoclonal cells, Golgi Zn^{2+} levels were unaffected, suggesting that they do not exert their role on α-syn PFF accumulation by modulating SLC39A9's function. Finally, Tau oligomers accumulation was unaffected in monoclonal *C3orf58* and *SLC39A9* KO cells (**Supplementary Figure 10**), and α-syn PFF accumulation

was decreased in *TM9SF2* KO and increased in *VPS35* heterozygous monoclonal cells (**Supplementary Figure 7C**, partially rescuable for VPS35), confirming our results on polyclonal KO populations (**Figure 2B, Figure 3E**).

C3orf58 and SLC39A9 regulate binding of α-syn-PFF to the cell surface

To further investigate the role of SLC39A9 and C3orf58 in mediating α-syn PFF accumulation, we compared the transcriptome of both KO lines to that of WT cells using RNAseq **(Figure 5E-G**, **Supplementary Figure 11**, **Tables S7, S8)**. Strikingly, both KO lines showed highly similar transcriptomic changes, sharing 83% of their top 100 differentially expressed genes (**Figure 5E**), and 606 in total **(Supplementary Figure 11A-C)** with highly comparable magnitude of changes (**Figure 5F**, correlation coefficient R^2=0.979). Accordingly, PCA and clustering analysis indicated clear distinction between KO and WT samples, with both KO genotypes indistinguishable from each other **(Supplementary Figure 11D,E)**. The top 15 affected GO terms based on differential gene expression were also shared (**Figure 5G**). This indicated that these two genes might act in (a) similar(s) pathway(s) mediating PFF accumulation. The GO analysis pointed towards major changes at the plasma membrane and in the extracellular matrix (**Figure 5G**), suggesting that the uptake/endocytosis of α-syn PFF might be impaired by loss of *SLC39A9* and *C3orf58*, rather than PFF clearance being increased. We thus monitored PFF uptake at early time points (15 min, 2 h) in WT, *C3orf58* KO, *SLC39A9* KO and rescued cells using fluorescence microscopy. The trypsinization step preliminary to cell fixation allows the removal of PFF that are bound to the cell surface but not yet internalized (**Supplementary Figure 12A**, PBS wash vs Trypsin wash). Image analyses revealed that both the percentage of PFF-positive cells and the median fluorescence intensity were severely reduced in *C3orf58* KO and *SLC39A9* KO cells, which could be rescued by WT constructs, slightly less by kinase-dead C3orf58, and not at all by Zn^{2+} transport-deficient SLC39A9 H185R **(Supplementary Figure 12B,C,D)**. These results clearly establish that *C3orf58* and *SLC39A9* deficiencies reduce PFF uptake by impairing early steps of internalization. Since RNAseq indicated that the plasma membrane composition might be altered in *C3orf58* and *SLC39A9* KO cells, we investigated whether the binding of α-syn PFF to the cell surface was affected **(Figure 6A,B)**. PFF binding was greatly reduced by loss of *C3orf58* or *SLC39A9* and rescued by expression of WT proteins but not the SLC39A9 H185R mutant. Taken together, our transcriptomic data suggest that C3orf58 or SLC39A9 deficiency may significantly alter the plasma membrane and extracellular matrix composition, leading to decreased binding of α-syn PFF to the cell surface.

We then tested whether this could be due to changes in specific proteins exposed at the cell surface of KO cells by surveying the surface proteome. We used a biotin-containing compound to label surface proteins (**Supplementary Figure 13A, B**)[49], and identified labeled proteins by streptavidin pulldown followed by LC-MS/MS (**Table S9**). No significant changes were observed in the surface proteome of *C3orf58* and *SLC39A9* KO cells, nor in *VPS35* heterozygous cells (**Supplementary Figure 13C, D, F**). *TM9SF2* KO cells had elevated levels of NID2 (nidogen-2) and LOXL1 (lysyl oxidase homolog 1) (**Supplementary Figure 13E**), two proteins the homolog of which may interact together in other species[50,51] and regulate cell-extracellular matrix interactions[52]. Since TM9SF2 deficiency affected not only α-syn PFF, but also Tau oligomers uptake (**Figure 3D, E**), we did not pursue this further. Together, our data suggest that C3orf58 and SLC39A9 deficiencies do not modulate α-syn PFF binding by perturbing the cell surface proteome, although it cannot be excluded that lower abundance proteins not detected in our proteomics analysis are affected.

C3orf58 and SLC39A9 regulate HS homeostasis

Several lines of evidence suggested that alteration of HS homeostasis might explain the decreased PFF binding at the cell surface of *SLC39A9* and *C3orf58* deficient cells. First, HS seem to mediate most of PFF binding to the cell surface in RPE-1 cells based on genetic evidence from the screen and loss of PFF binding upon heparinases or sodium chlorate treatment (**Figure 4**). Second, RNAseq indicated changes at the cell surface including "glycosaminoglycan binding" in both KOs (**Figure 5G**). Third, post-fixation staining of HS expression estimated by IF against the 10e4 epitope showed decreased HS in *SLC39A9* KO cells and C3orf58 overexpressing cells (resc. WT line) (**Supplementary Figure 7A, B**).

To further characterize the regulation of HS expression by *SLC39A9* and *C3orf58*, we performed surface HS labeling in parallel to the PFF binding assay (**Figure 6**). Quantification indicated a severe loss of sulfated HS signal in *SLC39A9* KO cells (**Figure 6A, C**), which was rescued by SLC39A9 WT but not the H185R mutant. *C3orf58* KO cells, despite having lower PFF binding capacity, displayed similar HS signals to WT cells (**Figure 6A, C**). Surprisingly, upon rescue with C3orf58 WT, PFF binding was restored despite an overall decreased 10e4 antibody reactivity and regardless of the highly variable N-sulfated HS signal in individual cells. In the C3orf58 3MUT rescue line, restored PFF binding was not accompanied by a decrease in HS staining. Interestingly, at higher magnification, puncta of PFF bound to the cell surface of *C3orf58* KO cells showed reduced colocalization with sulfated HS puncta, phenocopying sodium chlorate treatment (**Supplementary Figure 14**, **Figure 4C**). Again, the C3orf58 3MUT rescue line behaved differently, with only a partial restoration of colocalization.

Our RNAseq analysis provided another piece of evidence suggesting perturbed HS homeostasis in *C3orf58* KO and *SLC39A9* KO cells. **Supplementary Figure 15** shows significant modulations of some HS biology relevant genes that were similar between the two lines, including changes in HS core proteins genes (*SDC3*, *GPC1*, *GPC6*), in HS biosynthetic enzymes (*EXT1*, *NDST1*, *NDST3*, *HS2ST1*, *HS3ST1*, *HS3ST3A1*, *HS3ST3B1*, *XYLT1*). An increase in the chondroitin sulfate core protein gene *CSPG4* indicated a possible more general dysregulation of glycosaminoglycan metabolism.

These data suggest that *SLC39A9* and *C3orf58* may both play a role in HS biosynthesis and/or modification, resulting in decreased PFF binding upon loss of either gene, but in a way that maintains sulfated HS detection using the 10e4 antibody in *C3orf58* KO cells, a staining that is unlikely to recapitulate the complexity and diversity of HS chains.

Alterations in expression and composition of surface HS in C3orf58 and SLC39A9 deficient cells revealed by LC-MS/MS analysis

These results prompted us to analyze into more detail HS expression and modification using LC-MS/MS to quantify HS disaccharides and tetrasaccharides species purified from WT, *C3orf58* KO and *SLC39A9* KO cells, and rescued counterparts. When combined, total HS species were significantly increased in *C3orf58* KO cells in a rescuable manner (**Figure 7A, B, E**). This was true for many disaccharides and tetrasaccharides species, including the increase in the most abundant species (ΔUA-GlcNAc, ΔUA-GlcNS, **Figure 7F, G**; see other species in **Supplementary Figure 16**). On the other hand, total HS were slightly decreased in *SLC39A9* KO cells compared to WT, but not significantly (p=0.198), which was also rescued (**Figure 7A, E**). This was again driven by a significant decrease in the most abundant disaccharides exposed at the surface of WT RPE-1 cells (ΔUA-GlcNAc, ΔUA-GlcNS, ΔUA2S-GlcNS, **Figure 7A ,B, F-H**, as well as ΔUA2S-GlcNAc, **Supplementary Figure 16**). Beyond absolute amount of total HS and individual species, their relative abundance in HS chains (i.e. HS composition) is an important parameter that determines ligand binding capacities[28]. Contrary to the significant increase in many HS species observed

in *C3orf58* KO cells, their overall HS disaccharide and tetrasaccharide composition was unchanged except for a slight increase in ΔUA2S-GlcNAc (**Figure 7C, D**; **Supplementary Figure 16**). However, HS composition was strongly affected in C3orf58 rescued lines, consistent with a possible implication of this protein in HS homeostasis, as suggested by the decreased HS 10e4 signal in C3orf58 resc. WT cells and reduced PFF binding in *C3orf58* KO cells (**Figure 6, Supplementary Figure 7A, B**).

SLC39A9 KO cell surface HS composition was severely affected. An increase, although not reaching significance, was observed for the unmodified ΔUA-GlcNAc disaccharide, while a decrease was observed for the other abundant disaccharides ΔUA-GlcNS, ΔUA2S-GlcNS (**Figure 7C, D**; **Supplementary Figure 16**). This pattern of HS composition with an increased ratio of unmodified disaccharides coupled to a decrease in N-sulfated species, was highly similar to that observed in C3orf58 resc. WT cells and consistent with decreased 10e4 antibody signal in intact and permeabilized cells (**Figure 6, Supplementary Figure 7A, B**). Altogether, our analysis of cell surface HS abundance and composition reveals changes that can explain the binding of the 10e4 antibody, but not the PFF binding phenotype. However, they also confirm that both C3orf58 and SLC39A9 are important players in HS expression and composition, given that changes observed in the KO lines were rescued, and that overexpression of C3orf58 impacts HS composition.

ER-Golgi dynamics have been shown to regulate the localization of HS-modifying enzymes[53]. Thus we monitored whether Golgi structure was affected in *C3orf58* and *SLC39A9* KO cells by using a modified Golgi morphology analysis pipeline[54] (**Supplementary Figure 17**). Golgi area was increased in both lines in a rescuable manner. Both CisGolgi and transGolgi were larger in *SLC39A9* KO cells, while only the CisGolgi increase in area reached significance in *C3orf58* KO cells (**Supplementary Figure 17B**). Other parameters (compactness, CisGolgi and transGolgi markers signal intensities, and number of fragments) were unchanged (**Supplementary Figure 17C-F**). Whether perturbed Golgi morphology is sufficient to explain changes in HS homeostasis and the PFF uptake phenotype remains to be determined.

C3orf58 is an important player for PFF uptake in human iPSC-derived microglia

Finally, we tested whether *C3orf58* and *SLC39A9* are important for α-syn PFF uptake in a PD-relevant cell type. We generated *C3orf58* and *SLC39A9* KO human induced pluripotent stem cells (iPSC) using CRISPR/Cas9 (**Figure 8A**, **Supplementary Figure 18A-C**). Pluripotency, genome stability and karyotype of the lines were verified (**Figure 8A**, **Supplementary Figure 18D-F**). These cells differentiated adequately into microglia (iMGL) as indicated by their morphology, qRT-PCR and FACS-based quantification of microglial markers (**Figure 8A**, **Supplementary Figure 19**). WT, *C3orf58* KO or *SLC39A9* KO iMGL were treated with fluorescent α-syn PFF uptake and a trypan blue washing step allowed to visualize only internalized fibrils. High-content microscopy-based imaging and quantification were performed (**Figure 8B, C**) and revealed that *C3orf58* KO reduced PFF uptake by approximately 60% in iMGL, while *SLC39A9* KO did not have a significant effect. This data shows that *C3orf58* is required for α-syn PFF uptake in a PD-relevant cell type.

DISCUSSION

In this study, we sought to identify key molecular mechanisms and genes involved in the intracellular uptake of α-syn PFF. We used a genome-wide unbiased approach in a neuroepithelial cell line, RPE-1 cells, and identified genes affecting HSPGs as major factors in α-syn PFF binding to the cell surface and subsequent uptake in recipient cells. All the validated hits were specific for proteinaceous aggregates (α-syn PFF or tau oligomers), with *C3orf58* and *SLC39A9* being highly specific to α-syn PFF. These two genes could thus be of particular interest for the treatment of synucleinopathies, because targeting their activity might have less secondary effects than HSPG in general, given the many biological functions HSPG exert. In the initial screen, FACS sorting for enrichment of cells with higher or lower PFF accumulation was performed solely based on labeled PFF fluorescence, without accounting for cell size. In retrospect, we clearly showed that PFF content was correlated to cell size, and that silencing of genes that modify the growth or division of cells can be a major confounding factor in such FACS-based screens **(Figure 1, 2** and **Supplementary Figure 2)**. These data will help other researchers in the design of studies with similar approaches in the future, especially given the effect of CRISPR/Cas9 genome editing on cell cycle[55]. Another limitation in our study pertains to the shorter time allowed for obtaining a polyclonal perturbed cell population in our validation phase compared to the screen itself before PFF treatment (3 days vs 9 days, respectively). Thus, it is possible that our validation phase contains false negatives that could have shown an effect at later time points. This includes genes that have previously been linked with our key identified pathways: *SLC10A7* deficiency alters HS expression[31], while TMED10 has been attributed a role in unconventional targeting of proteins in the ER-Golgi intermediate compartment[56] and to act as a cargo receptor for COPI mediated Golgi to ER retrograde transport[57]. TMED10 has also been proposed to regulate macropinocytosis through an unclear mechanism[58], plasma membrane v-ATPase (several subunits of which were targeted in the low PFF population of our screen) is also able to control macropinocytic events[59] and VPS35 can localize to maturating macropinosomes[60]. Macropinocytosis is involved in PFF uptake in RPE-1 cells, since treatment with the macropinocytosis inhibitor EIPA strongly reduced PFF accumulation (**Supplementary Figure 20**), but also in other cell types including Hela cells, iPSC-derived astrocytes and dopaminergic neurons[19]. Validation in monoclonal KO cells of additional hits may reveal new players and better delineate their molecular interplay in key pathways necessary for PFF uptake in the future.

For feasibility purposes, we used a 24 h PFF treatment paradigm in the screen, which did not allow to directly conclude whether uptake or removal of PFF was affected, and we thus use the term "accumulation" when appropriate. Quantification of early uptake events, before significant degradation by the cellular machinery can occur, and PFF binding assays performed in the cold allowed to confirm the involvement of *C3orf58* and *SLC39A9* in the adhesion of PFF to the cell surface. Given *i)* the magnitude of uptake inhibition in cells KO for either gene **(Figure 5D)** and *ii)* the extremely similar changes in transcriptomic profiles in KO cells **(Figure 5E-G and Supplementary Figure 11)**, this strongly suggests that both genes affect (a) similar pathway(s) which deregulation leads to largely decreased PFF binding to the cell surface **(Figure 6)**. We provide several lines of evidence suggesting HSPG biosynthesis and maturation are commonly regulated by both genes. First, the HSPG biosynthetic enzymes EXT1 and NDST1 were extremely significant hits in our screen **(Figure 1B)** and their effect on PFF uptake was very strong in the validation phase **(Figure 2B)**. Second, in RPE-1 cells, PFF binding to the cell surface was very severely affected by pre-treatments that stripped off or decreased sulfation of HSPG **(Figure 4)**. Third, KO of the Golgi PAPS transporters *SLC35B2*/*SLC35B3* strongly reduced PFF uptake (**Supplementary Figure 5**).

Fourth, KO of *C3orf58* phenocopied sodium chlorate treatment on HSPG signals and the colocalization between HSPG and PFF bound to the cell surface **(Figure 4; Figure 6; Supplementary Figure 14A,B; 13)**. Fifth, both *C3orf58* and *SLC39A9* KO lines displayed changes in HSPG related genes **(Supplementary Figure 15)** and perturbations in HS quantity or composition at the cell surface **(Figure 7, Supplementary Figure 16)**. Finally, *C3orf58* and *SLC39A9* have both been identified in genome-wide CRISPR screens as cellular factors regulating infection by viruses that depend on HS for cellular entry (*C3orf58*, Zika virus[42]; *SLC39A9*, Chikungunya virus[38]).

In contrast to binding of tau aggregate to HS which relies on specific N- and 6-O sulfation, it appears that no specific sulfate moiety, but rather global sulfation levels, are necessary for α-syn PFF binding and uptake[25,35]. We confirm these findings, since we did not find specific changes in di-/tetra-saccharide unit at the cell surface of *C3orf58* and *SLC39A9* KO cells that correlated with changes in α-syn PFF binding/uptake (**Figure 7, Supplementary Figure 16**). The observation that KO of *NDST1* is sufficient to greatly decrease PFF uptake (**Figure 2B, Figure 3E**) is insufficient to conclude that N-sulfation is the sole necessary modification for HS/PFF interaction, since NDST1 activity is likely largely influencing other downstream HS modifications. HS di-/tetra-saccharide composition is likely not providing the adequate resolution of HS determinants for α-syn binding, as changes in total amount but not composition were observed at the surface of *C3orf58* KO cells. HS chains are arranged as alternating domains of varying number of disaccharides in length, either enriched in N-sulfated (NS, 6 to 16 units) or N-Acetylated (NAc, up to 18 units), or containing a mix of NAc/NS. HS-binding proteins can bind one or two domains simultaneously[28]. Future analyses using synthetic, structurally defined oligosaccharides are likely to uncover the specific arrangements that are necessary to allow α-syn PFF binding to HS chains. Even though we cannot exclude that one or several proteins might be needed as secondary receptors, our data suggests that at least in RPE-1, HS are the major receptor for α-syn PFF binding to the cell surface.

C3orf58 and *SLC39A9* may act as general regulators of glycans/glycosaminoglycans biosynthesis and/or maturation in the Golgi. This would be consistent with the previously reported decrease in complex-type N-glycans and O-glycans (due to decreased C1GalT1 expression) in *SLC39A9* KO cells[61]. B4GalT4 and C1GalT1 are both Mn^{2+}-dependent galactosyl transferases, a class of enzymes which activity is decreased upon increased Zn^{2+}/Mn^{2+} ratio[62]. Zn^{2+} levels are increased in the Golgi of SLC39A9 KO cells (**Supplementary Figure 9** and ref[46]), possibly explaining the effects on N- and O-glycosylations[61]. More generally, it is possible that SLC39A9 acts as general regulator of the activity of Golgi-resident, Mn^{2+}-dependent enzymes, by decreasing the local Zn^{2+} concentration. Thus, C3orf58 and SLC39A9 could both play a role in regulating glycans biosynthesis, including glycosaminoglycan like HS and chondroitin sulfate (CS), thereby shaping a cell surface environment that is competent for α-syn PFF binding and uptake. This is compatible with the observed changes in expression of HS and CS related genes in our transcriptomic analysis **(Supplementary Figure 15)**. HS enzymes are subjected to both anterograde and retrograde trafficking via COPII and COPI vesicles respectively. Brefeldin-A treatment, which inhibits COPI-mediated retrograde transport, causes mislocalization of HS-modifying enzymes (including NDST1) from the cis- to the transGolgi[53]. Given the previously reported colocalization of C3orf58 with the β-COP subunit of the COPI, it can be hypothesized that retrograde trafficking is compromised in *C3orf58* KO cells. Altered trafficking of glycosyltransferases including HS biosynthetic enzymes may also occur in *TM9SF2* KO cells, since TM9SF2 was previously shown to affect HS surface expression by affecting proper localization and stability of NDST1[38], possibly explaining its effect as a Zika virus host factor[63]. Whether

trafficking defects of HS biosynthetic enzymes in *C3orf58* and/or *SLC39A9* KO cells are at the basis of their role in HS homeostasis remains to be determined.

Interestingly, despite a report that a murine microglial cell line (BV-2) only slightly relies on HSPG for α-syn PFF uptake, with heparinase treatment only decreasing uptake by 25%[25], we have found that loss of the HSPG-regulating *C3orf58* gene in human iPSC-derived microglia decreased PFF uptake by 60% (**Figure 8**). This difference might be due to the various origin of microglial cells used, or to the possibility that *C3orf58* might regulate additional processes in microglia besides HSPG maturation. For instance, function or expression of MerTK, a surface receptor tyrosine kinase necessary for non-inflammatory homeostatic phagocytosis in microglia that is necessary for efficient α-syn PFF uptake in human microglia[64], might be altered upon *C3orf58* deficiency. Alternatively, an interplay between MerTK and HSPGs can be envisioned, since HSPGs have been reported previously to act as accessory molecules to influence receptor tyrosine kinase activation[65]. The importance of *C3orf58,* and of HSPG in general, for PFF uptake in other human iPSC-derived PD-relevant cell types is under investigation (astrocytes, dopaminergic neurons, dopaminergic neural progenitor cells). Validation of this effect *in vivo* will be an important milestone in the validation of *C3orf58* as a potential therapeutic target to prevent the spreading of α-syn aggregates in synucleinopathies.

MATERIAL AND METHODS

Production of lentiviral particles and transduction

For lentiviral production, 293T cells were transfected with constructs of interest (in the pLJM1 plasmids, lentiCas9-Blast plasmid, or pCW57.1 NDST1-HA plasmid) together with packaging plasmids (pMD2.g, pMDLg/pRRE, pRSV-Rev) using the Calcium Phosphate method. A medium change with fresh medium supplemented with non-essential amino acids mix (Wisent) was performed after 8 hours of transfection. The lentivirus-containing supernatant was harvested 48 hours post-transfection, filtered with a 0.45 µm filter, and recipient RPE-1 cells were transduced with a range of virus quantity before selection with 15 µg/ml puromycin (or 2 µg/mL blasticidin for Cas9). Wells where complete selection resulted in 70-90% cell death compared to untransduced control were chosen to ensure that most surviving cells statistically received only one lentiviral copy. These were kept as stable cell lines.

Cell culture

Retina Pigmented Epithelial (RPE-1) and HEK 293T cells were maintained in DMEM containing 4.5 g/l glucose, sodium pyruvate, 10% fetal bovine serum and penicillin/streptomycin. Cells were passaged by rinsing in PBS followed by incubation in trypsin/EDTA (Wisent, 325-542-EL) at 37°C for approximately 5 minutes before resuspension in complete medium to inactivate trypsin. Cells were counted with a Luna cell counter (Logos Biosystems). The cell suspension was then seeded in recipient culture vessels at the desired cell density. All transgenes expressed in RPE-1 cells were delivered by lentiviral transduction. The macropinocytosis inhibitor EIPA (A3085, 5-(N-Ethyl-N-isopropyl)amiloride, Sigma) was dissolved in methanol, which was used as a vehicle control. Alexa488 EGF complex (E13345, ThermoFisher) was used at 120 ng/mL, Alexa488-conjugated transferrin (T13342, ThermoFisher) was used at 20 µg/mL, and Oregon Green 488-conjugated dextran (70,000 MW, D7172, ThermoFisher) was used at 100 µg/mL.

iPSC culture and generation of *C3orf58* -/- or *SLC39A9* -/- iPSC

iPSC cultures were grown at 37°C, 5% CO2 for 2 weeks in supplemented mTeSR medium (STEMCELL Technologies #85850). For KO of *C3orf58* or *SLC39A9* in iPSC, iPSC cultures were grown at 37°C, 5% CO2 for 2 weeks in supplemented mTeSR medium. Cells were then nucleofected with two synthetic guide RNAs per targeted gene (Synthego) as indicated in **Supplementary Figure 19A** and **Table S4**, as described previously[66]. Polyclonal KO cell populations were recovered and genes KO were confirmed by genomic DNA extraction and PCR. To obtain monoclonal lines, polyclonal cell populations were dissociated and individual cells sorted by flow cytometry, and plated as single cells. Single clones were screened for gene KO by PCR and sequencing (**Supplementary Figure 19B,C**) and pure monoclonal cultures were selected, amplified and stored for further use. Staining for pluripotency markers, qPCR for genome stability assessment, and karyotyping were performed as described previously[67].

Differentiation of iPSCs into dopaminergic neurons

Cells were then grown in suspension for a week in uncoated flasks in induction medium: DMEM F12 (Gibco #10565-018) containing 1x N-2 supplement (Gibco #17502048), 1x B-27 supplement (Gibco #17504044), 1x MEM NEAA solution, 1 mg/mL BSA, 200 ng/mL Noggin, 200 ng/mL SHH (C24II), 3 µM CHIR-99021, 10 µM SB431542 and 100 ng/mL FGF-8. After a week, iPSC formed embryoid bodies (EBs) which were plated in induction medium onto dishes coated with Poly-L ornithine and laminin (PO/L). Attached EBs were kept for another week in culture, then dissociated into small aggregates and plated

again onto new PO/L coated flasks in induction medium. At this stage, cells differentiated into early dopaminergic neural progenitor cells (DA NPCs) and were kept in induction medium for another week. DA NPCs were then dissociated into a single cell suspension and plated in final dishes in differentiation medium: BrainPhys™ Neuronal Medium containing 1x N2A supplement and 1xSM1 supplement (STEMCELL Technologies #05793) as well as 20 ng/mL BDNF, 20 ng/mL GDNF, 1 µg/mL laminin, 200 µM ascorbic acid, 0.1 µM Compound E and 0.5 mM Dibutyryl-cAMP. After 2 weeks in culture in final differentiation medium, TH positive dopaminergic neurons were observed.

Differentiation of iPSCs into microglia (iMGL), quality control, and PFF uptake

Differentiation of iPSCs into iMGL was carried out following a previously established protocol[68]. Briefly, hematopoietic progenitor cells were generated from iPSCs using STEMdiff Hematopoietic kit (STEMCELL Technologies) and cultured in microglia growth medium supplemented with 100 ng/mL interleukin-34, 50 ng/mL tumor growth factor-beta and 25 ng/mL macrophage colony-stimulating factor (Peprotech) for 25 days, following which 100 ng/mL cluster of differentiation 200 (Abcam) and C-X3-C motif chemokine ligand 1 (Peprotech) were also added to the culture. iMGL were considered mature after 28 days of differentiation. Cells were maintained at 37°C under a 5% CO_2 atmosphere throughout the protocol. For qRT-PCR control of differentiation status, TRIzol (ThermoFisher Scientific) was used to extract RNA, followed by cleaning using a RNeasy mini kit (Qiagen). Reverse transcription was performed using Moloney murine leukemia virus reverse transcriptase (ThermoFisher Scientific). Real-time PCR was performed using TaqMan assays (ThermoFisher Scientific) on a QuantStudio™ 5 real-time PCR system (ThermoFisher Scientific). The $2^{-\Delta Ct}$ method was used to analyze the data using glyceraldehyde 3-phosphate dehydrogenase (GAPDH) and tyrosine 3-monooxygenase/tryptophan 5-monooxygenase activation protein zeta (YWHAZ) as controls.

For quality control of differentiation by FACS, cells were blocked with Human TrueStain FcX and TrueStain Monocyte Blocker (Biolegend) and stained with the following antibodies: anti-CSF1R (clone #61708, R&D Systems), anti-CX3CR1 (clone #2A9-1, Biolegend), anti-MERTK (clone #125518, R&D Systems). Appropriate forward and side scatter profiles were used to exclude debris and doublets from the analysis. Dead cells were excluded based on LIVE/DEAD™ Fixable Aqua (ThermoFisher Scientific) staining. Readings were done on an Attune™ Nxt Flow Cytometer and analyzed/visualized using FlowJo™ software.
For PFF uptake assay, Cells were challenged with 250 nM Alexa Fluor 488-labelled PFFs for three hours and then washed once with 4% trypan blue solution to quench extracellular fluorescence, and twice with PBS. Cells were fixed in 4% paraformaldehyde solution and counterstained with Hoechst 33342 (1 µg/mL). Total green fluorescence intensity per cell was quantified using a CellInsight CX5 High Content Screening Platform (ThermoFisher Scientific). All conditions were assessed in triplicate.

In silico structural modeling

The superposition and cartoons were generated using PyMOL v2.4. The AlphaFold2 model[69] coordinates were retrieved from Uniprot (accession numbers Q8NDZ4 and Q9NUM3 for C3orf58 and SLC39A9 respectively). Structural homologs of both proteins were identified using FoldSeek[70]. For C3orf58, the most similar PDB100 structure with a nucleotide in the active site was WNK1 (pdb 5TF9)[71], with a probability score of 0.98. For SLC39A9, the most similar PDB100 structure was the Zrt-/Irt-like ZIP protein from Bordetella bronchiseptica with bound Zn^{2+} (pdb 5TSA)[72], with a probability score of 1.00.

Genome-wide CRISPR screen

$250x10^6$ RPE-1 cells were transduced in a 1,000 mL suspension to which was added the lentiviral library-containing supernatant (to reach <0.3 MOI based on previously performed titration) and polybrene (final concentration 8 µg/mL). Cells were then plated in 15 cm dishes at a density of $5x10^6$ cells per plate. The medium was changed 24 h after plating. 48 h after plating, cells were trypsinized, and replated in medium containing 15 µg/mL puromycin. A fifth of a plate of library transduced cells was also seeded in absence of puromycin to compare its growth to selected cells and extrapolate the actual MOI at the end of selection. One plate of untransduced cells was also treated with puromycin to determine the time necessary for completion of selection. After 3 days of selection, all library-treated cells (with and without puromycin) were trypsinized and counted, and the MOI was determined to be 0.18, indicating that a vast majority of transduced cells has received only one lentiviral particle. The library-treated, puromycin-selected cells were plated again in 15 cm dishes at $5x10^6$ cells per dish. After 3 days, cells were plated in new 15 cm dishes ($5x10^6$ cells/dish) and separated in two replicates of $150x10^6$ cells each for future PFF-A633 treatment. For each replicate, 3 additional plates (3x $5x10^6$ cells) were also seeded to serve as untreated (no PFF) controls, i.e. baseline representation of sgRNAs in the total population. 24 h after seeding, plates from both replicates were treated independently with 15 nM PFF-A633 in complete medium. After 24 h, cells were harvested by trypsinization, pooled by repetitive centrifugation, counted, and split in 5x 15 mL tubes containing $30x10^6$ cells each (>$150x10^6$ cells per replicate). These were spun down and gently resuspended in 4 % PFA/PBS (pH 7.4, 10 mL/$30x10^6$ cells) by slowly vortexing. After a 15 min incubation on a rotator, cells were spun down, and rinsed 3 times in PBS by repetitive resuspension/centrifugation. The cell suspensions were kept in 5 mL PBS at 4°C in the dark before proceeding to triage by FACS. A population of RPE-1 cells transduced with a lentivirus encoding Cas9 and a LacZ-targeting sgRNA was subjected to the same treatments as the lentiviral library-transduced population (transduction, selection, and treatment with or without PFF-A633), to use as gating controls in FACS sorting.

The cells with the 15 % lowest and 15 % highest PFF-A633 fluorescence were sorted by FACS. Briefly, cell suspensions were adjusted to $30x10^6$ per 2 mL and dispensed in 5mL FACS tubes with cell strainer snap cap (Corning, 352235). Replicate 1 was sorted on FACS Aria II and replicate 2 on a BD Influx System. In tota, $10x10^6$ to $13x10^6$ cells per sample were obtained after sorting, providing 138-fold library coverage. The sorted cells for each population (replicate 1 – Low pFF/High PFF ; replicate 2 – Low PFF/High PFF) were pooled, centrifuged, and the cell pellet was kept at -80°C before gDNA extraction.

Genomic DNA (gDNA) extraction from fixed cells

A custom protocol was used for gDNA extraction from fixed cells, as follows, and scaled proportionally for each sample depending on actual cell counts. In a 15 mL conical tube, 6 mL of NK lysis Buffer (50 mM Tris, 50 mM EDTA, 1% SDS, pH 8.0, sterile water) and 30 µL of 20 mg/mL Proteinase K (Qiagen, 19131) were added to the $30x10^6$ cells, and incubated at 55°C 30 min, inverted and gently vortexed, then incubated again at 55°C overnight. The next day, 30 µL of 10 mg/mL RNAse A (Qiagen, 19101, diluted in NK lysis buffer to 10 mg/mL and then stored at 4°C) was added to the lysed sample, which was then inverted 25 times and incubated at 37°C for 30 min. Samples were cooled on ice before addition of 2 mL pre-chilled 7.5 M ammonium acetate (Sigma A1542) to precipitate proteins. Stock solutions of 7.5M ammonium acetate was made in sterile dH_2O and kept at 4°C until use. After adding ammonium acetate, the samples were vortexed at high speed for 20 seconds followed by centrifugation at > 4,000 g for 10 min. After the spin, a tight pellet was visible in each tube and the supernatant was carefully decanted

into a new 15 mL canonical tube. 6 mL of 100 % isopropanol was then added to the tube, inverted 50 times, and centrifuged at >4,000 g for 10 min. gDNA was visible as a small white pellet in each tube. The supernatant was discarded, 6 mL of freshly prepared 70 % ethanol was added, the tube was inverted 10 times, and then centrifuged at >4,000 g for 1 min. The supernatant was discarded by pouring, the tube was briefly spun, and remaining ethanol was removed using a P200 pipette tip. After air drying for 10-30 min, the DNA changed appearance from a milky white pellet to slightly translucent. At this stage, 500 µL of 1x TE buffer (Sigma, T9285) was added, the tube was incubated at 65°C for 1 h and at room temperature overnight to fully resuspend the DNA. The next day, the gDNA samples were vortexed briefly. The gDNA concentration was measured using a Nanodrop (Thermo Scientific), and gDNA concentration was adjusted to 400 ng/µL in 1X Tris-EDTA buffer.

sgRNA sequences libraries preparation, Illumina sequencing and analysis with MAGeCK

For the first (outer) PCR, an approximately 107-fold library coverage was obtained by performing 21 reactions (50 µL each) per sample of the following PCR recipe: 2.5 µg gDNA, 10 µM Outer primers (see **Table S5**), 2X KAPA HiFi HotStart ReadyMixPCR Kit, ultrapure water q.s.p. 50 µL. All reactions for a given sample were pooled and mixed by vortexing, and 50 µL per sample were run on 2 % agarose gel to check for the presence of a faint ~600 bp amplicon. The second (inner) barcoding PCR was performed as shown in **Table S5** for unique barcoding of each sample. Each PCR product was then run on a 2 % agarose gel until good separation between that barcoding PCR amplicon (~200 bp) was well separated from the ~600 bp outer PCR amplicon. The barcoding PCR amplicon was gel extracted for each sample, DNA was quantified using a Nanodrop, the A260/A280 ratio checked for sample quality, and samples were stored at -20°C before pooling and Illumina sequencing. The number of reads obtained for each sample is indicated in **Table S5**. Raw sequencing data will be made available publicly.

Validation of screen hits by high-content microscopy

Lentiviral particles encoding Cas9 (blasticidin selection) and EGFP (puromycin selection) were used sequentially to generate RPE-1 cells stably expressing Cas9 and EGFP. These cells were then used for gene editing by reverse transfection in 96 wells plates for imaging. Briefly, each well received 5.6 µL of a 3 µM synthetic sgRNA solution, to which was added 25 µL of a HiPerFect (Qiagen, 301705) transfection mix (0.75 µL HiPerFect + 24.25 µL serum-free DMEM). After 10 min incubation at room temperature, 2,000 cells were seeded per well (100 µL of a 20,000 cells/mL suspension in complete DMEM) before incubation at 37°C. This brought the sgRNA concentration to app. 130 nM final. A full medium change was performed after 24 h of transfection. After 72 h of transfection, cells were treated with 15 nM PFF-A633 for 24 h before rinsing 3x with PBS, followed by 20 min fixation in 4 % paraformaldehyde (PFA) at room temperature. Cells were rinsed again in PBS, nuclei were stained with Hoechst 33342 (Invitrogen, H3570) for 10 min (0.2 µg/ml in PBS), and after 2x rinsing in PBS, cells were imaged using a CX7 high-content microscope. Image analysis was performed using the HCS Studio Cell Analysis software. Briefly, cells were defined as objects using the thresholded EGFP channel, and the cell area quantified as the EGFP-positive area (in pixels) for each cell. The integrated PFF-A633 signal per cell was also quantified using the thresholded PFF-A633 channel. The ratio of PFF-A633 signal over cell area was then calculated for each cell. The mean value of PFF signal/cell area was calculated for each well, normalized as percentage of the mean of AAVS1 sgRNAs-treated wells, and used to create the final heatmap in GraphPad PRISM. sgRNAs sequences used are shown in **Table S4**.

Generation of monoclonal CRISPR-edited RPE-1 cells

RPE-1 cells stably expressing Cas9 were reverse transfected using HiPerFect in 24 well plates with synthetic sgRNAs against the target genes (*C3orf58*, *SLC39A9*, *TM9SF2*, *VPS35*). The method used was as described in the "validation of screen hits by high-content microscopy" section, except that all volumes and cell numbers were scaled up 6 times, and a combination of two sgRNAs was used, respecting the final sgRNAs concentration. sgRNAs sequences used are shown in bold in **Table S4.** 72 h post transfection, cells were trypsinized and resuspended. App. 25 % of the suspension was used for gDNA extraction (QuickExtract, Lucigen, QE09050) and validation of gene editing by PCR, assuming that efficient cleavage by both sgRNAs results in loss of a portion of the amplicon (*C3orf58*, *TM9SF2*, *VPS35*), or of one of the two reverse primers binding sites (*SLC39A9*). The rest of the suspension was used to isolate single cells in individual wells of 96 wells plates by FACS, and monoclonal lines were then amplified, screened by PCR, and gene editing validated by allelic sequencing. See Supplementary Figure 5 for PCR screening and allelic sequencing strategies.

Molecular cloning and plasmids

The lentiCas9-Blast plasmid (Addgene #52962, kind gift from Feng Zhang) was used to generate RPE-1 cells constitutively expressing Cas9. pLJM1-EGFP (puromycin selectable, Addgene #19319, gift from David Sabatini) was used to drive constitutive expression of EGFP in RPE-1-Cas9 cells. The pLJM1 backbone (derived from pLJM1-EGFP) was used to drive constitutive expression of all other constructs. The coding sequence of wild-type (WT) C3orf58 (codon optimized) and WT SLC39A9, both tagged with a C-terminal HA epitope, were ordered as gBlock gene fragments (Integrated DNA Technologies) and cloned into the NheI/EcoRI restriction sites of pLJM1 using Gibson Assembly (New England Biolabs (NEB)). The HA-tagged C3orf58-3MUT was generated by first introducing the D287N mutation using a mutated gBlock and the same cloning strategy as WT C3orf58. The additional K198A and D306N were then introduced using the QuikChange II site-directed mutagenesis kit (Agilent). The same kit was used to generate the HA-tagged D159A and H185R SLC39A9 mutants. The WT and D620N VPS35-HA constructs were PCR amplified from WT and D620N VPS35-6G-GFP constructs (in pAAV-GFP-CAG vector, kind gifts from Austen Milnerwood) and cloned into the NheI/EcoRI restriction sites of pLJM1 using Gibson Assembly. Doxycycline inducible NDST1-HA was PCR amplified from a home-made plasmid containing the human NDST1 cDNA fused to a C-terminal HA tag (pLJM1 NDST1-HA), before cloning into the NheI and BamHI sites of the pCW57.1 plasmid (Addgene #41393, gift from David Root) using T4 DNA ligase (NEB). All PCRs were made using Q5 DNA polymerase (NEB). All constructs were sequence verified. The sequence of oligonucleotides and dsDNA gene fragments used for cloning are indicated in **Table S5**.

Antibodies

Antibodies used in this study are listed in **Table S6**.

PFF uptake and binding assays, and live staining of surface heparan sulfate

For PFF binding assays, cells grown to 50-75% confluency on 96 well plates (Falcon, #353219) were placed on ice for 3 min, and rinsed once with cold unsupplemented DMEM. Cells were then incubated with 180 nM Alexa fluor-labeled PFFs and 10e4 anti-heparan sulfate antibody (1/500) in unsupplemented DMEM for 20 min on ice. After rinsing 3 times in cold DMEM, cells were fixed in cold 4 % PFA/PBS for 15 min, rinsed 3 times in PBS at room temperature (RT), and incubated for 25 min at RT in blocking solution (5% Normal Goat Serum in PBS). Finally, cells were incubated with Alexa fluor-coupled anti-mouse secondary antibody (ThermoFisher, 1/1000) and Hoechst 33342 (0.2 µg/ml) in blocking

solution for 20 min and rinsed 3 times in PBS before imaging on a Zeiss fluorescence microscope. Cells were plated at least 24 hours before starting the assays. Where indicated, cells were pre-treated at 37°C with sodium chlorate (Sigma, 403016-100G) in complete medium for 48 h, or for 1 h in serum-free DMEM with a cocktail of heparinase I (NEB, P0735S), heparinase II (NEB, P0736S) and heparinase III (NEB, P0737S) at 3 U/mL each.
For PFF uptake assays in RPE-1 cells, adherent cells were subjected to a medium change with culture medium containing Alexa-dyes coupled PFFs (15 nM in the FACS-based screen, or 60 nM for subsequent microscopy experiments) before overnight incubation at 37°C. Cells were then rinsed three times with PBS, before further processing.

PFF pulse-chase assay for early uptake

RPE-1 cells of the indicated genotypes were incubated on ice with 180 nM α-syn PFF-A633 for 20 min in serum-free DMEM. Cells were then incubated at 37°C for the indicated times, before a 30 sec wash with either PBS or pre-warmed trypsin to remove surface-bound PFFs and retain only signal of internalized PFFs. Cells were then fixed, and nuclei stained with Hoechst 33342 before imaging on a Zeiss epifluorescence microscope at 20x. Image quantification was performed using ImageJ.

Cell surface proteome labeling

The optimal concentration of EZ-Link™ Sulfo-NHS-Biotin reagent (21331, ThermoFisher) to be used for staining a maximum of cell surface proteins without labeling the interior of the cells was determined by microscopy (**Supplementary Figure 13A,B**). 8,000/well WT RPE-1 cells were plated in 96 wells plates for imaging and incubated at 37°C for 24 hours. All subsequent steps until fixation were performed at 4°C. Cells were then rinsed twice with ice-cold PBS containing Ca^{2+} and Mg^{2+} (311-011-CL, Wisent), then incubated for 30 min in 70 µL biotinylation solution consisting of EZ-Link™ Sulfo-NHS-Biotin reagent diluted at the indicated concentrations in PBS. After rinsing twice with PBS, remaining biotinylation reagent was inactivated by addition of 100 µL 100 mM glycine in PBS for 15 min before fixation in 4% PFA for 15 min. Then, cells were incubated for 1 h at room temperature in a PBS solution containing 0.2 µg/mL Hoechst 33342 (H3570, ThermoFisher) and 1 µg/mL Streptavidin-Alexa488 (016-540-084, Jackson ImmunoResearch). After 3 rinses with PBS, cells were imaged and analyzed using a CX7 high-content microscope.

For MS, one 10 cm plate per sample of ~90% confluent RPE-1 cells was used. For each line (WT, C3orf58$^{-/-}$, SLC39A9$^{-/-}$, TM9SF2$^{-/-}$, VPS35$^{+/-}$), biological triplicates were analyzed. All steps were performed in the cold until freezing cell pellets. Cells were washed twice with 7mL PBS Ca^{2+}/ Mg^{2+} before incubation with 7mL 0.25mg/mL EZ-Link™ Sulfo-NHS-Biotin in PBS for 30min, then washed twice with 7mL PBS. The remaining biotinylation reagent was inactivated by addition of 7mL 100mM glycine in PBS for 15min before 2 additional washes in 7mL and 4mL PBS. Cells were then scraped in 1mL PBS, and pelleted by centrifugation at 5,000g for 5min at 4°C. Supernatant was removed, and pellets snap frozen for 3min in a slurry of dry ice/70% ethanol. Pellets were frozen at -80C until processed.

Mass-spectrometry analysis of cell surface proteome

Lysis buffer containing 10 mM Tris-HCl, 150mM NaCl, 1% Triton, 0.1% SDS and 1mM protease inhibitor cocktail was added to the frozen pellet for 30min at 4C. Lysates were sonicated for 5 seconds and centrifuged at 4C for 30min at 4000rpm. Cleared lysates were incubated with 70 µl of streptavidin beads (5 ml; 17-5113-01, GE Healthcare) at 4° for 3 h, washed with lysis buffer followed by six washes using

50 mM ammonium bicarbonate (AB0032, 500G, Biobasic). For protein digestion, 0.2 µg of Trypsin/Lys C (V5071, Promega) was added into each 100 µl sample in 50 mM ammonium bicarbonate overnight at 37 °C. Supernatants were transferred into new microtubes, beads were washed two times with 100 µl of water and supernatants from all washes were pooled with the initial supernatant. Trifluoroacetic acid (1%; 302031 Sigma) was added to each tube to acidify samples. Samples were then desalted using desalting spin columns (89852; Pierce, ThermoFisher) per the manufacturer's protocol and subsequently dried in a SpeedVac. Peptides were resuspended in 26 µl of 1% formic acid and kept at –80 °C. Peptides were loaded onto a 75-µm internal diameter × 150 mm Self-Pack C18 column installed in an Easy-nLC 1000 system (Proxeon Biosystems). LC-MS/MS was conducted using a 120 min reversed-phase buffer gradient running at 250 nl/min (column heated to 40 °C) on a Proxeon EASY-nLC pump in-line with a hybrid LTQ-Orbitrap velos mass spectrometer (ThermoFisher Scientific). A parent ion scan was performed in the Orbitrap, using a resolving power of 60000. Simultaneously, up to the twenty most intense peaks were selected for MS/MS (minimum ion count of 1000 for activation) using standard CID fragmentation. Fragment ions were detected in the LTQ. Dynamic exclusion was activated such that MS/MS of the same m/z (within a 10 ppm window, exclusion list size 500) detected three times within 45 s were excluded from analysis for 30 s.

For protein identification, Raw MS files were analyzed using the Mascot search engine through the iProphet pipeline integrated into Prohits and the Human RefSeq database v.57. Search parameters specified a parent MS tolerance of 15 ppm and an MS/MS fragment ion tolerance of 0.4 Da, with up to two missed cleavages allowed for trypsin. Oxidation of methionine was allowed as a variable modification. Data were analyzed using the trans-proteomic pipeline[73] via the ProHits software suite[74]. Proteins identified with a ProteinProphet cut-off of 0.85 (corresponding to ≤1% FDR) were analyzed.

RNAseq analysis

RNAseq analysis was performed using the GenPipes RNAseq analysis pipeline version 3.0 run on Compute Canada's high performance computing cluster. The raw sequencing (FASTQ) files were aligned to the human genome version GRCh38 using STAR, Picard and Cufflinks were run for corrections and calculating raw and normalized RNA read counts. Differential gene expression was calculated using EdgeR[75]. Biological triplicates for control cultures were separately compared with triplicate samples of *C3orf58*$^{-/-}$ and *SLC39A9*$^{-/-}$ lines. P values were adjusted using a false rate discovery (FDR) correction for multiple comparisons and threshold 0.1 was applied to select differential expressed genes. The selected genes were the inputs into gene ontology analysis using GOseq[76].

Microscopy

Except for high-content microscopy analyses, microscopic analysis was performed as described previously[77].

Immunocytochemistry

Unless otherwise stated, cells previously plated in 96 wells plates for imaging were rinsed in PBS, fixed for 15 min in 4 % PFA/PBS, rinsed 3 times in PBS, permeabilized for 5 min with 0.15 % Triton X-100/PBS (or 0.05% NP-40 where indicated), rinsed again 3 times in PBS, and incubated for 30 min in blocking solution (5 % normal goat serum in PBS). After blocking, cells were incubated with the antibodies of interest for 1 h in blocking solution, rinsed 3 times in blocking solution, and incubated for 1 h with the adequate fluorescently-labeled secondary antibodies diluted in blocking buffer. Cells were rinsed 3 times

in PBS, incubated for 10 min with Hoechst 33342 (0.2 µg/mL) in PBS, and rinsed again 2 times before microscopy.

Western blot

Unless otherwise stated, samples were prepared for SDS-PAGE in 1X Laemmli buffer supplemented with 0.1M DTT and boiled for 10 min at 95°C. After separation by SDS-PAGE, proteins were transferred to Nitrocellulose membranes using the semi-dry Trans-Blot Turbo system (Bio-Rad). Membranes were then blocked in 5% milk/PBS-T (PBS containing 0.1% Tween 20), and primary antibodies were incubated in 1% milk/PBS-T by shaking at 4°C overnight. After 3 rinses in PBS-T, membranes were incubated with appropriate secondary antibodies coupled to horseradish peroxidase (Jackson ImmunoResearch) for 1 hour at room temperature, and rinsed again 3 times in PBS-T. HRP signal was revealed using ECL substrate (Pierce, or Bio-Rad's Clarity Max), and chemiluminescent signal was captured using a ChemiDoc imaging system (Bio-Rad).

Sodium carbonate extraction

RPE-1 cells grown to 80-90% confluency in a 35mm dish were rinsed twice with ice-cold PBS, scraped in 1 mL PBS and spun down at 5,000 g for 5 min at 4°C. The cell pellet was resuspended in 100 µL PBS, and proteins were quantified by BCA assay (Pierce). An amount of cell suspension representing 80 µg proteins was spun down again and resuspended in 80 uL (1 µg/µL protein) freshly prepared, cold 0.1 M Na_2CO_3 (pH 11.5). After 20 min incubation on ice, the suspension was ultracentrifuged at 100,000 rpm for 20 min at 4°C. The supernatant containing soluble and membrane associated proteins was supplemented with Laemmli buffer (1X final, 100 mM DTT). The pellet containing integral membrane proteins was resuspended in an equal volume of 1X Laemmli buffer containing 100 mM DTT. Samples were then boiled for 10 min at 95°C and processed for Western blot.

Measurement of Zn^{2+} content with Zinpyr-1

2,500 RPE-1 cells per well were seeded in 96 wells plates for imaging. The day after, cells were incubated at 37°C for 30 min with complete DMEM containing 5 µM Zinpyr-1 (Abcam, ab145349), Hoechst 33342 (0.2 µg/mL) and 1 mM EDTA. Cells were then washed twice in pre-warmed Live Cell Imaging Solution (ThermoFisher, A14291DJ) containing 1 mM EDTA, live cells were imaged with a CX7 high-content microscope connected to a live module (37°C, 5% CO_2, 60% humidity), and the mean average intensity per cell was quantified with the HCS Studio Cell Analysis software.

Purification of recombinant α-syn

The full-length human wild-type α-syn coding sequence was cloned into pGEX-6P-1 plasmid and then transformed into *E.coli* BL-21(DE3) strain. Bacteria were then grown in 500 mL of LB broth supplemented with ampicillin (100 µg/mL) expression of GST-tagged α-syn was induced by addition of 0.3mM IPTG. Bacteria were harvested by centrifugation at 5,000 g, 4°C for 15 min, resuspended in 30 mL of 25mM Tris-HCl (pH 8.0)-buffered solution containing 400 mM NaCl, 5% (v/v) glycerol, 0.5% (v/v) Triton-X100, 1mM DTT and protease inhibitor cocktails (0.5 µg/mL aprotonin, 0.5 µg/mL leupeptin, 130 µg/mL phenylmethylsulfonyl fluoride, 500 µg/mL benzamidine), and sonicated on ice-bath. The cell lysate was clarified by centrifugation at 20,000 g, 4°C for 30 min and added to a 50-mL Falcon tube holding 6mL of Glutathione-Sepharose® 4B resin (GE Healthcare) that was pre-equilibrated in the same buffer. This mixture was incubated on a nutator at 4°C overnight before packing onto a 10 mL disposable

polypropylene column. GST-α-syn bound to the resin was then eluted from the column with 20 mM glutathione freshly prepared in 25 mM Tris, 400 mM NaCl solution (pH 8.0). After combining all GST-α-syn eluates, protein concentration was determined using Bradford assay kit with BSA as a standard (Pierce). Based on the quantification result, GST-HRV 3C protease was added to GST-α-syn at a ratio of 1:50 (w/w) and the cleavage reaction was incubated at 4°C overnight to remove the GST tag from GST-α-syn. The reaction mixture was then concentrated to about 4 mL using Amicon Ultra-15 Centrifugal Filter Unit 3000 NMWL (Millipore) with multiple buffer exchanges to PBS (pH 7.4). The sample was subsequently loaded onto a PBS-equilibrated Superdex 200 16/600 column (GE Healthcare) on the ÄKTA Pure system. Fractions containing α-syn were collected and further purified by passing through a GSTrap 4B column (GE Healthcare). The purified α-syn was determined to be homogeneous by SDS-PAGE followed by Coomassie blue staining and the concentration was adjusted to 5 mg/mL in PBS (pH 7.4). Finally, the purified α-syn was sterile-filtered though a 0.22 µm PVDF syringe filter (Millipore) before being aliquoted and stored at -80°C.

Preparation of α-syn Pre-formed Fibrils (PFFs)

PFFs were prepared by shaking 0.5 mL aliquots of purified α-syn (5 mg/mL, so 346 µM equivalent monomers of 14.46 kDa α-syn) held in a 1.5 mL microtube on a ThermoMixer (Eppendorf) set at 1000 rpm and 37°C for 5 days. The obtained fibrils were sonicated to produce smaller species of fibrillated α-syn (i.e. PFFs) on a Bioruptor® Plus sonication unit (Diogenode) with cooling water circulation at 10°C for 30 sec x 10 cycles. Samples (~20 µL) were harvested before and after sonication for quality control by electron microscopy imaging and dynamic light scattering analysis. For electron microscopy, PFFs were characterized using a negative staining protocol. PFFs were added to 200 mesh cupper carbon grid (SPI Supplies, 3520C-FA), fixed 1 min with 4% paraformaldehyde and stained with 2% uranyl acetate (EMS, 22400-2) for 1 min. PFFs were visualized using a transmission electron microscope (FEI Tecnai 12 Bio Twin 120kV TEM) coupled to an AMT XR80C CCD Camera (**Supplementary Figure 1A**). The length of individual fibrils was measured with ImageJ and the size distribution analyzed with MATLAB. PFFs were of 54.24 nm average length after sonication (**Supplementary Figure 1B**) The sonicated PFFs were either aliquoted (20 µL) for storage at -80°C or further labelled with fluorescent dyes as indicated below.

Preparation of fluorescent dye-labelled α-syn PFFs

Sonicated PFFs (150 µL) were gently mixed with 5 µL of Alexa Fluor® 633 or 488 succinimidyl ester dyes (5 mg/mL in DMSO) and incubated in the dark for 20 min at room temperature. The labelled product was then transferred to a Slide-A-Lyzer device (Thermo Scientific) and dialyzed against PBS (pH 7.4) at 4°C with three changes of dialysis buffer to remove the free residual fluorescent dye. 20µL aliquots were made prior to storage at -80°C. The concentration of the labeled PFFs was extrapolated from the initial concentration (5 mg/ml) and final volume post-dialysis.

Preparation of Cy3-labeled tau oligomers

Recombinant tau monomers (human 4R2N T40/ Evotec, Germany) were labeled with Cy3 (Life Technologies). To prepare tau oligomers, 5 µM monomeric tau in 100mM MES buffer (pH=6.5; 4-Morpholineethanesulfonic acid hydrate) was mixed with 10 µM DTT (BioShop) and incubated for 10 min at 55°C. Subsequently, 5 µM heparin (Fisher, H19) was added to the solution to induce aggregation and incubated with shaking (1000 rpm) for 4 h at 37°C. Tau oligomers were stored at -80°C.

Analysis of cell-surface Heparan Sulfate by LC-MS/MS

a) cell surface HS harvesting: 90% confluent RPE-1 cells in 15 cm dishes were rinsed twice in 10 mL PBS before detachment using 2mL trypsin/EDTA for 10 min at 37°C. 3 mL serum-free DMEM was added and the cell suspension was triturated before harvesting in a 15 mL conical tube, ensuring minimal left-over cell suspension in the plate. The suspension was centrifugated for 3 min at 2,000 rpm. The supernatant containing HS (detached from the cell surface after trypsin digestion of HSPG) was carefully removed from the pellet and frozen at -80°C and shipped on dry ice before analysis. The cell pellet was also frozen at -80°C before protein quantification using DC protein assay (Bio-Rad).

b) sample preparation for LC-MS/MS: A DEAE column was applied to purify the HS from post-trypsinization cell supernatants. Before loading to DEAE column, 2 µL ^{13}C-labeled recovery calibrant NSK5P (45 ng/µL) was added to cell supernatant. DEAE column mobile phase A contained 20 mM Tris, pH 7.5 and 50 mM NaCl, and mobile phase B contained 20 mM Tris, pH 7.5 and 1 M NaCl. After loading the sample into DEAE column, the column was washed with 1.5 mL mobile phase A, followed by 1.5 mL mobile phase B to elute the HS. The YM-3KDa spin column was applied to desalt the elute, and the retentate was subjected to heparin lyases digest. Before the digestion, ^{13}C-labeled 3-*O*-sulfated calibrants (each 500 ng) were added to the retentate. 100 µL of enzymatic buffer (100 mM sodium acetate/2 mM calcium acetate buffer (pH 7.0) containing 0.1 g/L BSA), and the 20 µL of enzyme cocktails containing 5 mg/mL each of heparin lyase I and II was added to degrade the retentate on the filter unit of the YM-3KDa column. The reaction solution was incubated at 37 °C for 6 h. Before recovering the disaccharides from the digest solution, a known amount ^{13}C-labeled non-3-*O*-sulfated disaccharide calibrants (ΔIS=80 ng, ΔIIS=80 ng, ΔIIIS=40 ng, ΔIVS=80 ng, ΔIA=40 ng, ΔIIA=80 ng, ΔIIIA=40 ng, ΔIVA=250 ng) were added to the digestion solution. The HS disaccharides and tetrasaccharides were recovered by centrifugation, and the filter unit was washed twice with 200 µL of deionized water. The collected filtrates were freeze-dried before the AMAC derivatization. The AMAC label and LC-MS/MS analysis of the collected disaccharides and tetrasaccharides was performed as described below. The amount of HS was determined by comparing the peak area of native di/tetra-saccharide to each corresponding ^{13}C-labeled internal standard, and the recovery yield was calculated based on a comparison of the amount of ^{13}C-labeled disaccharide (Δ[^{13}C]UA-[^{13}C]GlcNS from heparin lyases degraded ^{13}C-labeled NSK5P) in the tissue samples and control, respectively.

c) Chemical derivatization of HS disaccharides: The 2-Aminoacridone (AMAC) derivatization of lyophilized samples was performed by adding 10 µL of 0.1 M AMAC solution in DMSO/glacial acetic acid (17:3, v/v) and incubating at room temperature for 15 min. Then 10 µL of 1M aqueous sodium cyanoborohydride (freshly prepared) was added to this solution. The reaction mixture was incubated at 45 °C for 2 h. After incubation, the reaction solution was centrifuged to obtain the supernatant that was subjected to the LC-MS/MS analysis.

d) LC-MS/MS analysis: The analysis of AMAC-labeled di/tetra-saccharides was implemented on a Vanquish Flex UHPLC System (ThermoFisher Scientific) coupled with TSQ Fortis triple-quadrupole mass spectrometry as the detector. The ACQUITY Glycan BEH Amide column (1.7 µm, 2.1 × 150 mm; Waters, Ireland, UK) was used to separate di/tetra-saccharides at 60 °C. Mobile phase A was 50 mM ammonium formate in water, pH 4.4. Mobile phase B is acetonitrile. The elution gradient as follows: 0-20 min 83-60% B, 20-25 min 5% B, 25-30 min 83% B. The flow rate was 0.3 mL/min. On-line triple-quadrupole mass spectrometry operating in the multiple reaction monitoring (MRM) mode was used as the detector. The ESI-MS analysis was operated in the negative-ion mode using the following parameters: Neg ion spray voltage at 3.0 kV, sheath gas at 55 Arb, aux gas 25 arb, ion transfer tube temp at 250 °C and vaporizer temp at 400 °C. TraceFinder software was applied for data processing.

Golgi structure analysis

Immunocytochemistry was performed on RPE-1 cells of the indicated genotypes, using GM130 as a cisGolgi marker and Golgin97 as a transGolgi marker. Z-stacks (60 stacks per field, 0.185 µm steps) were acquired using a Nikon A1 confocal microscope mounted with a Plan Apo λ 60x 1.40 objective. Then, a customized CellProfiler pipeline largely inspired from Mejia et al.[54] was used to analyze Golgi morphology. Briefly, changes were made to the Mejia et al. pipeline so that cell outlines corresponded to nuclei extended by 17 pixels, and those that touched the image border were filtered out from analyses. Diameters of objects and thresholding factors were adjusted to ensure correct features detection. Fluorescence intensity measurement modules for GM130 and Golgin97 channels were added.

ACKNOWLEDGMENTS

We thank all members (present and past) from the Fon lab, the Early Drug Discovery Unit led by Thomas M. Durcan, and members of the Angers lab for helpful discussions and support throughout the study. We also thank the FACS facility of the Faculty of Medicine from the University of Toronto for their help in processing CRISPR screen samples. Special thanks to Peter S. McPherson and his lab members for sharing thoughts, material and reagents, and to Grégoire Bonnamour at the CERMO-FC microscopy platform for technical help.

COMPETING INTERESTS

JL is a founder and chief scientific officer of Glycan Therapeutics Corp. ZW is currently an employee of Glycan Therapeutics Corp. Other authors have no competing interest to declare.

REFERENCES

1. Jellinger, K. A. Synucleinopathies. in *Encyclopedia of Movement Disorders* (eds. Kompoliti, K. & Metman, L. V.) 203–207 (Academic Press, 2010). doi:10.1016/B978-0-12-374105-9.00291-4.
2. Wakabayashi, K. *et al.* Accumulation of alpha-synuclein/NACP is a cytopathological feature common to Lewy body disease and multiple system atrophy. *Acta Neuropathol* **96**, 445–52 (1998).
3. Masuda-Suzukake, M. *et al.* Prion-like spreading of pathological -synuclein in brain. *Brain* **136**, 1128–1138 (2013).
4. Goedert, M., Falcon, B., Clavaguera, F. & Tolnay, M. Prion-like mechanisms in the pathogenesis of tauopathies and synucleinopathies. *Curr. Neurol. Neurosci. Rep.* **14**, 495 (2014).
5. Li, J.-Y. *et al.* Lewy bodies in grafted neurons in subjects with Parkinson's disease suggest host-to-graft disease propagation. *Nat. Med.* **14**, 501–503 (2008).
6. Luk, K. C. *et al.* Exogenous alpha-synuclein fibrils seed the formation of Lewy body-like intracellular inclusions in cultured cells. *Proc. Natl. Acad. Sci. U. S. A.* **106**, 20051–20056 (2009).
7. Volpicelli-Daley, L. A. *et al.* Exogenous alpha-synuclein fibrils induce Lewy body pathology leading to synaptic dysfunction and neuron death. *Neuron* **72**, 57–71 (2011).
8. Luk, K. C. *et al.* Intracerebral inoculation of pathological alpha-synuclein initiates a rapidly progressive neurodegenerative alpha-synucleinopathy in mice. *J Exp Med* **209**, 975–86 (2012).
9. Luk, K. C. *et al.* Pathological alpha-synuclein transmission initiates Parkinson-like neurodegeneration in nontransgenic mice. *Science* **338**, 949–53 (2012).
10. Emmanouilidou, E. *et al.* Cell-produced alpha-synuclein is secreted in a calcium-dependent manner by exosomes and impacts neuronal survival. *J. Neurosci. Off. J. Soc. Neurosci.* **30**, 6838–6851 (2010).
11. Dieriks, B. V. *et al.* α-synuclein transfer through tunneling nanotubes occurs in SH-SY5Y cells and primary brain pericytes from Parkinson's disease patients. *Sci. Rep.* **7**, 42984 (2017).
12. Abounit, S. *et al.* Tunneling nanotubes spread fibrillar α-synuclein by intercellular trafficking of lysosomes. *EMBO J.* **35**, 2120–2138 (2016).
13. Danzer, K. M. *et al.* Heat-shock protein 70 modulates toxic extracellular α-synuclein oligomers and rescues trans-synaptic toxicity. *FASEB J.* **25**, 326–336 (2011).
14. Lee, J.-G., Takahama, S., Zhang, G., Tomarev, S. I. & Ye, Y. Unconventional secretion of misfolded proteins promotes adaptation to proteasome dysfunction in mammalian cells. *Nat. Cell Biol.* **18**, 765–776 (2016).
15. Oh, S. H. *et al.* Mesenchymal Stem Cells Inhibit Transmission of α-Synuclein by Modulating Clathrin-Mediated Endocytosis in a Parkinsonian Model. *Cell Rep.* **14**, 835–849 (2016).

16. Zhang, Q. *et al.* A myosin-7B–dependent endocytosis pathway mediates cellular entry of α-synuclein fibrils and polycation-bearing cargos. *Proc. Natl. Acad. Sci.* (2020) doi:10.1073/pnas.1918617117.
17. Hudák, A. *et al.* Contribution of syndecans to cellular uptake and fibrillation of α-synuclein and tau. *Sci. Rep*. **9**, 16543 (2019).
18. Holmes, B. B. *et al.* Heparan sulfate proteoglycans mediate internalization and propagation of specific proteopathic seeds. *Proc. Natl. Acad. Sci. U. S. A.* **110**, E3138-3147 (2013).
19. Bayati, A. *et al.* Rapid macropinocytic transfer of α-synuclein to lysosomes. *Cell Rep.* **40**, 111102 (2022).
20. Mao, X. *et al.* Pathological α-synuclein transmission initiated by binding lymphocyte-activation gene 3. *Science* **353**, (2016).
21. Birol, M., Wojcik, S. P., Miranker, A. D. & Rhoades, E. Identification of N-linked glycans as specific mediators of neuronal uptake of acetylated α-Synuclein. *PLOS Biol.* **17**, e3000318 (2019).
22. Cavaliere, F. *et al.* In vitro α-synuclein neurotoxicity and spreading among neurons and astrocytes using Lewy body extracts from Parkinson disease brains. *Neurobiol. Dis.* **103**, 101–112 (2017).
23. Rostami, J. *et al.* Human Astrocytes Transfer Aggregated Alpha-Synuclein via Tunneling Nanotubes. *J. Neurosci*. **37**, 11835–11853 (2017).
24. Freundt, E. C. *et al.* Neuron-to-neuron transmission of α-synuclein fibrils through axonal transport. *Ann. Neurol.* **72**, 517–524 (2012).
25. Ihse, E. *et al.* Cellular internalization of alpha-synuclein aggregates by cell surface heparan sulfate depends on aggregate conformation and cell type. *Sci. Rep.* **7**, 9008 (2017).
26. Sarrazin, S., Lamanna, W. C. & Esko, J. D. Heparan Sulfate Proteoglycans. *Cold Spring Harb. Perspect. Biol.* **3**, (2011).
27. Carlsson, P., Presto, J., Spillmann, D., Lindahl, U. & Kjellén, L. Heparin/Heparan Sulfate Biosynthesis PROCESSIVE FORMATION OF N-SULFATED DOMAINS. *J. Biol. Chem.* **283**, 20008–20014 (2008).
28. Xu, D. & Esko, J. D. Demystifying Heparan Sulfate–Protein Interactions. *Annu. Rev. Biochem.* **83**, 129–157 (2014).
29. Hart, T. *et al.* Evaluation and Design of Genome-Wide CRISPR/SpCas9 Knockout Screens. *G3 Bethesda Md* **7**, 2719–2727 (2017).
30. Li, W. *et al.* MAGeCK enables robust identification of essential genes from genome-scale CRISPR/Cas9 knockout screens. *Genome Biol.* **15**, 554 (2014).
31. Dubail, J. *et al.* SLC10A7 mutations cause a skeletal dysplasia with amelogenesis imperfecta mediated by GAG biosynthesis defects. *Nat. Commun.* **9**, 3087 (2018).

32. Di Mattia, T. *et al.* Identification of MOSPD2, a novel scaffold for endoplasmic reticulum membrane contact sites. *EMBO Rep.* **19**, (2018).
33. Zimprich, A. *et al.* A mutation in VPS35, encoding a subunit of the retromer complex, causes late-onset Parkinson disease. *Am. J. Hum. Genet.* **89**, 168–175 (2011).
34. Ansell-Schultz, A., Reyes, J. F., Samuelsson, M. & Hallbeck, M. Reduced retromer function results in the accumulation of amyloid-beta oligomers. *Mol. Cell. Neurosci.* **93**, 18–26 (2018).
35. Stopschinski, B. E. *et al.* Specific glycosaminoglycan chain length and sulfation patterns are required for cell uptake of tau vs. α-synuclein and β-amyloid aggregates. *J. Biol. Chem.* (2018) doi:10.1074/jbc.RA117.000378.
36. Park, J. S. *et al.* A FACS-Based Genome-wide CRISPR Screen Reveals a Requirement for COPI in Chlamydia trachomatis Invasion. *iScience* **11**, 71–84 (2019).
37. Woo, C. H. *et al.* Conserved function of the lysine-based KXD/E motif in Golgi retention for endomembrane proteins among different organisms. *Mol. Biol. Cell* **26**, 4280–4293 (2015).
38. Tanaka, A. *et al.* Genome-Wide Screening Uncovers the Significance of N-Sulfation of Heparan Sulfate as a Host Cell Factor for Chikungunya Virus Infection. *J. Virol.* **91**, (2017).
39. Tian, X. *et al.* DIPK2A promotes STX17- and VAMP7-mediated autophagosome-lysosome fusion by binding to VAMP7B. *Autophagy* **16**, 797–810 (2020).
40. Bareja, A., Hodgkinson, C. P., Payne, A. J., Pratt, R. E. & Dzau, V. J. HASF (C3orf58) is a novel ligand of the insulin-like growth factor 1 receptor. *Biochem. J.* **474**, 771–780 (2017).
41. Takatalo, M. S., Tummers, M., Thesleff, I. & Rönnholm, R. Novel Golgi Protein, GoPro49, Is a Specific Dental Follicle Marker. *J. Dent. Res.* **88**, 534–538 (2009).
42. Wells, M. F. *et al.* Genome-wide screens in accelerated human stem cell-derived neural progenitor cells identify Zika virus host factors and drivers of proliferation. *bioRxiv* 476440 (2018) doi:10.1101/476440.
43. Christianson, H. C. & Belting, M. Heparan sulfate proteoglycan as a cell-surface endocytosis receptor. *Matrix Biol.* **35**, 51–55 (2014).
44. Hart, T. *et al.* High-Resolution CRISPR Screens Reveal Fitness Genes and Genotype-Specific Cancer Liabilities. *Cell* **163**, 1515–1526 (2015).
45. Mani, K. *et al.* The heparan sulfate-specific epitope 10E4 is NO-sensitive and partly inaccessible in glypican-1. *Glycobiology* **14**, 599–607 (2004).

46. Matsuura, W. *et al.* SLC39A9 (ZIP9) regulates zinc homeostasis in the secretory pathway: characterization of the ZIP subfamily I protein in vertebrate cells. *Biosci. Biotechnol. Biochem.* **73**, 1142–1148 (2009).
47. Takagishi, T., Hara, T. & Fukada, T. Recent Advances in the Role of SLC39A/ZIP Zinc Transporters In Vivo. *Int. J. Mol. Sci.* **18**, (2017).
48. Dudkiewicz, M., Lenart, A. & Pawłowski, K. A novel predicted calcium-regulated kinase family implicated in neurological disorders. *PloS One* **8**, e66427 (2013).
49. Li, Y. *et al.* Sensitive profiling of cell surface proteome by using an optimized biotinylation method. *J. Proteomics* **196**, 33–41 (2019).
50. Pourhaghighi, R. *et al.* BraInMap Elucidates the Macromolecular Connectivity Landscape of Mammalian Brain. *Cell Syst.* **10**, 333-350.e14 (2020).
51. Abdelilah-Seyfried, S. *et al.* A gain-of-function screen for genes that affect the development of the Drosophila adult external sensory organ. *Genetics* **155**, 733–752 (2000).
52. Zhang, J.-L. *et al.* Vertebrate extracellular matrix protein hemicentin-1 interacts physically and genetically with basement membrane protein nidogen-2. *Matrix Biol. J. Int. Soc. Matrix Biol.* **112**, 132–154 (2022).
53. Meneghetti, M. C. Z. *et al.* ER-Golgi dynamics of HS-modifying enzymes via vesicular trafficking is a critical prerequisite for the delineation of HS biosynthesis. *Carbohydr. Polym.* **255**, 117477 (2021).
54. Mejia, I., Chen, Y.-C. & Díaz, B. Analysis of Golgi Morphology Using Immunofluorescence and CellProfiler Software. in *Golgi: Methods and Protocols* (eds. Wang, Y., Lupashin, V. V. & Graham, T. R.) 765–784 (Springer US, 2023). doi:10.1007/978-1-0716-2639-9_46.
55. Haapaniemi, E., Botla, S., Persson, J., Schmierer, B. & Taipale, J. CRISPR–Cas9 genome editing induces a p53-mediated DNA damage response. *Nat. Med.* **24**, 927 (2018).
56. Zhang, M. *et al.* A Translocation Pathway for Vesicle-Mediated Unconventional Protein Secretion. *Cell* **181**, 637-652.e15 (2020).
57. Nickel, W., Sohn, K., Bünning, C. & Wieland, F. T. p23, a major COPI-vesicle membrane protein, constitutively cycles through the early secretory pathway. *Proc. Natl. Acad. Sci.* **94**, 11393–11398 (1997).
58. Luteijn, R. D. *et al.* A Genome-Wide Haploid Genetic Screen Identifies Heparan Sulfate-Associated Genes and the Macropinocytosis Modulator TMED10 as Factors Supporting Vaccinia Virus Infection. *J. Virol.* **93**, e02160-18 (2019).

59. Ramirez, C., Hauser, A. D., Vucic, E. A. & Bar-Sagi, D. Plasma membrane v-ATPase controls oncogenic Ras-induced macropinocytosis. *Nature* **576**, 477–481 (2019).
60. Buckley, C. M. *et al.* WASH drives early recycling from macropinosomes and phagosomes to maintain surface phagocytic receptors. *Proc. Natl. Acad. Sci.* **113**, E5906–E5915 (2016).
61. Yamaji, T. *et al.* A CRISPR Screen Using Subtilase Cytotoxin Identifies SLC39A9 as a Glycan-Regulating Factor. *iScience* **15**, 407–420 (2019).
62. Prabhu, A., Gadre, R. & Gadgil, M. Zinc supplementation decreases galactosylation of recombinant IgG in CHO cells. *Appl. Microbiol. Biotechnol.* **102**, 5989–5999 (2018).
63. Li, Y. *et al.* Genome-wide CRISPR screen for Zika virus resistance in human neural cells. *Proc. Natl. Acad. Sci.* **116**, 9527–9532 (2019).
64. Dorion, M.-F. *et al.* MerTK is a mediator of alpha-synuclein fibril uptake by human microglia. *Brain* awad298 (2023) doi:10.1093/brain/awad298.
65. Lanzi, C. & Cassinelli, G. Receptor tyrosine kinases and heparan sulfate proteoglycans: Interplay providing anticancer targeting strategies and new therapeutic opportunities. *Biochem. Pharmacol.* **178**, 114084 (2020).
66. Deneault, E. *et al.* A streamlined CRISPR workflow to introduce mutations and generate isogenic iPSCs for modeling amyotrophic lateral sclerosis. *Methods San Diego Calif* **203**, 297–310 (2022).
67. Chen, C. X.-Q. *et al.* A Multistep Workflow to Evaluate Newly Generated iPSCs and Their Ability to Generate Different Cell Types. *Methods Protoc.* **4**, 50 (2021).
68. McQuade, A. *et al.* Development and validation of a simplified method to generate human microglia from pluripotent stem cells. *Mol. Neurodegener.* **13**, 67 (2018).
69. Jumper, J. *et al.* Highly accurate protein structure prediction with AlphaFold. *Nature* **596**, 583–589 (2021).
70. van Kempen, M. *et al.* Fast and accurate protein structure search with Foldseek. *Nat. Biotechnol.* 1–4 (2023) doi:10.1038/s41587-023-01773-0.
71. Yamada, K. *et al.* Discovery and Characterization of Allosteric WNK Kinase Inhibitors. *ACS Chem. Biol.* **11**, 3338–3346 (2016).
72. Zhang, T. *et al.* Crystal structures of a ZIP zinc transporter reveal a binuclear metal center in the transport pathway. *Sci. Adv.* **3**, e1700344 (2017).
73. Pedrioli, P. G. A. Trans-proteomic pipeline: a pipeline for proteomic analysis. *Methods Mol. Biol. Clifton NJ* **604**, 213–238 (2010).

74. Liu, G. *et al.* ProHits: integrated software for mass spectrometry-based interaction proteomics. *Nat. Biotechnol.* **28**, 1015–1017 (2010).
75. Robinson, M. D., McCarthy, D. J. & Smyth, G. K. edgeR: a Bioconductor package for differential expression analysis of digital gene expression data. *Bioinforma. Oxf. Engl.* **26**, 139–140 (2010).
76. Young, M. D., Wakefield, M. J., Oshlack, A. & Smyth, G. K. goseq: Gene Ontology testing for RNA-seq datasets.
77. Alcalay, R. N. *et al.* SMPD1 mutations, activity, and α-synuclein accumulation in Parkinson's disease. *Mov. Disord.* **34**, 526–535 (2019).

Figure 1. –CRISPR/Cas9 screening identifies genetic modifiers of α-syn PFF accumulation in RPE-1 cells

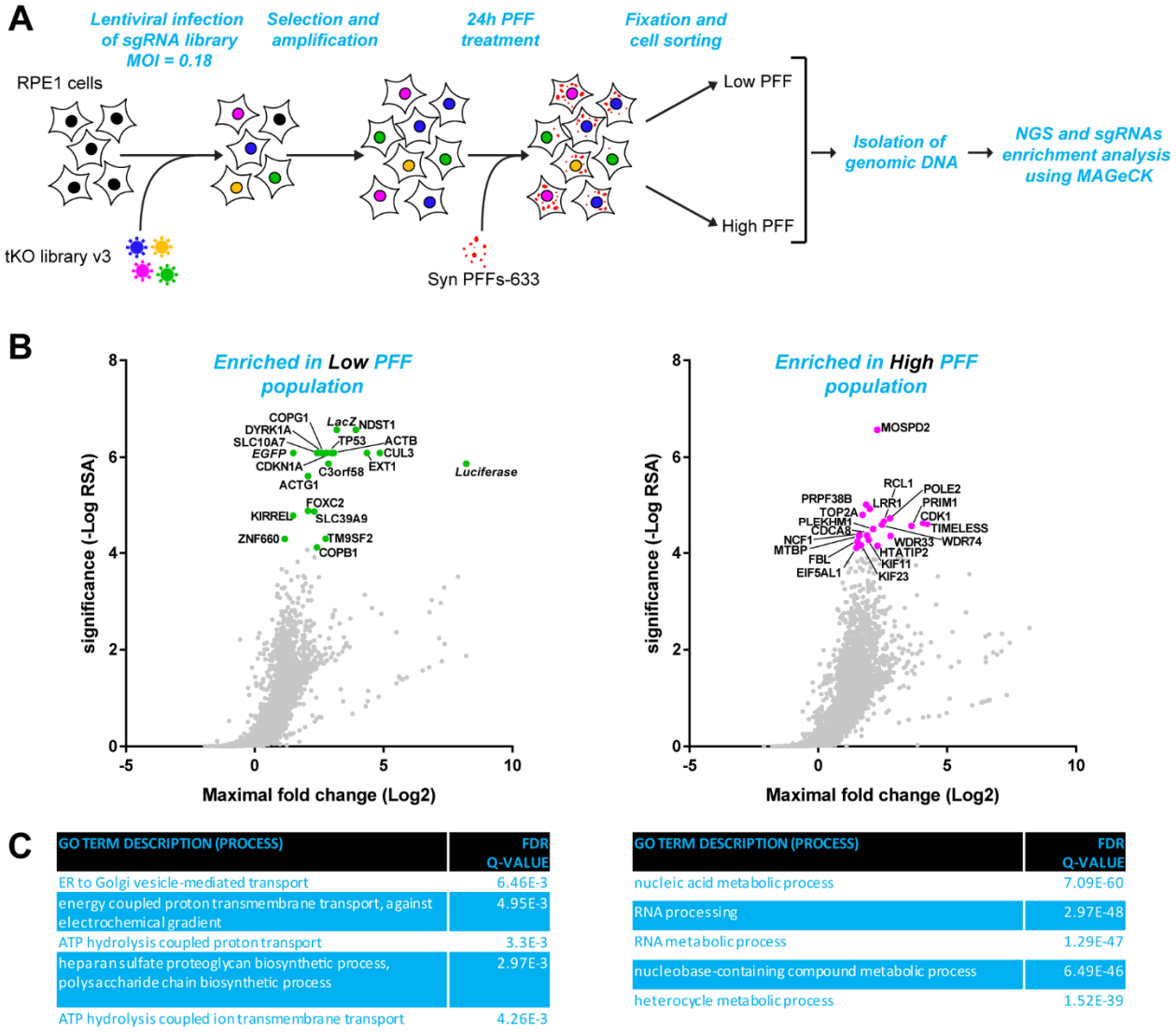

C

GO TERM DESCRIPTION (PROCESS)	FDR Q-VALUE
ER to Golgi vesicle-mediated transport	6.46E-3
energy coupled proton transmembrane transport, against electrochemical gradient	4.95E-3
ATP hydrolysis coupled proton transport	3.3E-3
heparan sulfate proteoglycan biosynthetic process, polysaccharide chain biosynthetic process	2.97E-3
ATP hydrolysis coupled ion transmembrane transport	4.26E-3

GO TERM DESCRIPTION (PROCESS)	FDR Q-VALUE
nucleic acid metabolic process	7.09E-60
RNA processing	2.97E-48
RNA metabolic process	1.29E-47
nucleobase-containing compound metabolic process	6.49E-46
heterocycle metabolic process	1.52E-39

(A) Strategy of the genome-wide CRISPR screening used to identify genetic modifiers of α-syn-PFFs accumulation in RPE-1 cells. FACS-sorting was used to isolate the cell populations with the 15% lower and 15 % higher PFF fluorescence intensity. **(B)** sgRNA enrichment in the Low PFF population (left panel) and High PFF population (right panel) was calculated using the MAGeCK algorithm. For all genes in the tKOv3 library, the significance (reproducibility of effect across all 4 sgRNAs for a given gene) was plotted as a function of the maximal Log2 fold change (sgRNA showing the highest enrichment for that gene). The top 20 most significant genes are shown as green or magenta dots, and the associated gene symbols are indicated. **(C)** Gene ontology (GO) analysis was performed with the GOrilla online tool, with the ranked lists of genes from the MAGeCK analysis as inputs (Low PFF population, left ; High PFF population, right). The enriched GO terms for the Process category and their associated false-discovery rate Q-values are reported in the tables.

Figure 2. – Screen validation by high-content microscopy

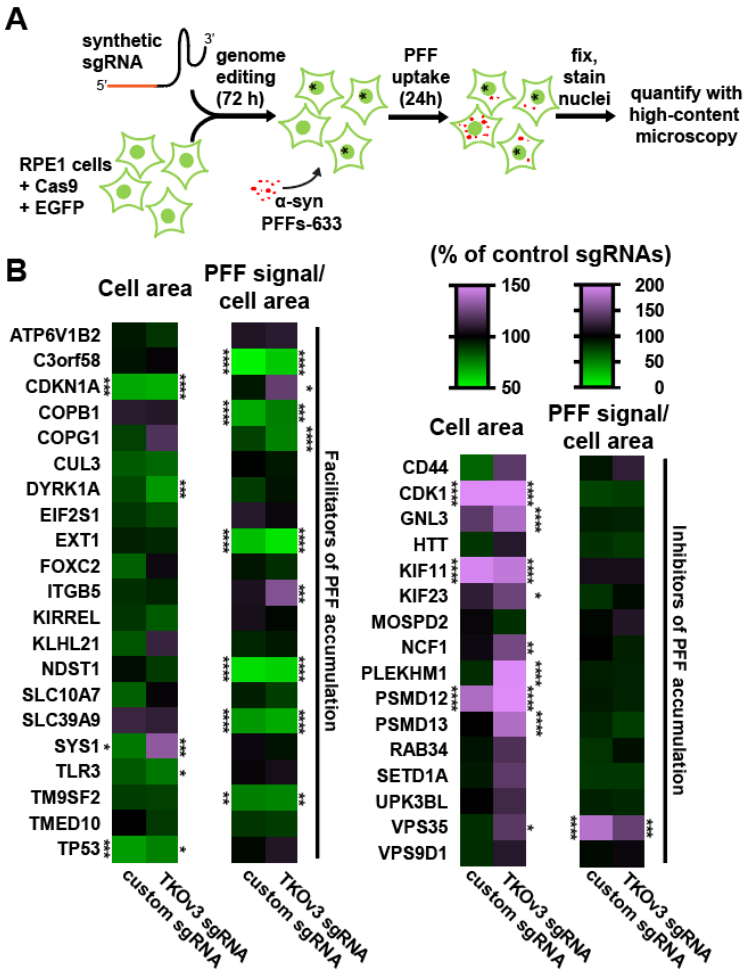

(A) Experimental pipeline used for hits validation by high-content microscopy. RPE-1 cells stably expressing Cas9 nuclease and EGFP are transfected with individual synthetic sgRNAs in 96 wells plates. After 3 days, the obtained polyclonal gene-edited cells are subjected to a 24 h α-syn-PFF-A633 uptake assay before fixation, nuclei stain with Hoechst and quantification by high-content microscopy. An EGFP mask allows quantification of cell area, to which PFF content is normalized. Imaging was done using a CX7 high-content microscope and quantification with the HCS Studio Cell Analysis software. **(B)** Heatmap summarizing validation data. On a per cell basis, the EGFP area and PFF-A633/cell area ratio were measured, for each indicated gene, and for two sgRNAs per gene (a custom sgRNA and one from the tKOv3 library). The mean cell area and mean PFF-A633/cell area were calculated and reported as percent of control sgRNAs targeting the AAVS1 locus (see color coding at the bottom left). Genes symbols are sorted alphabetically, with putative hits enriched in the Low PFF population first, followed by putative hits enriched in the High PFF population. Statistical test: one-way ANOVA ; * $p<0.05$, ** $p<0.01$, *** $p<0.001$, **** $p<0.0001$.

Figure 3. – Cargo specificity of validated hits

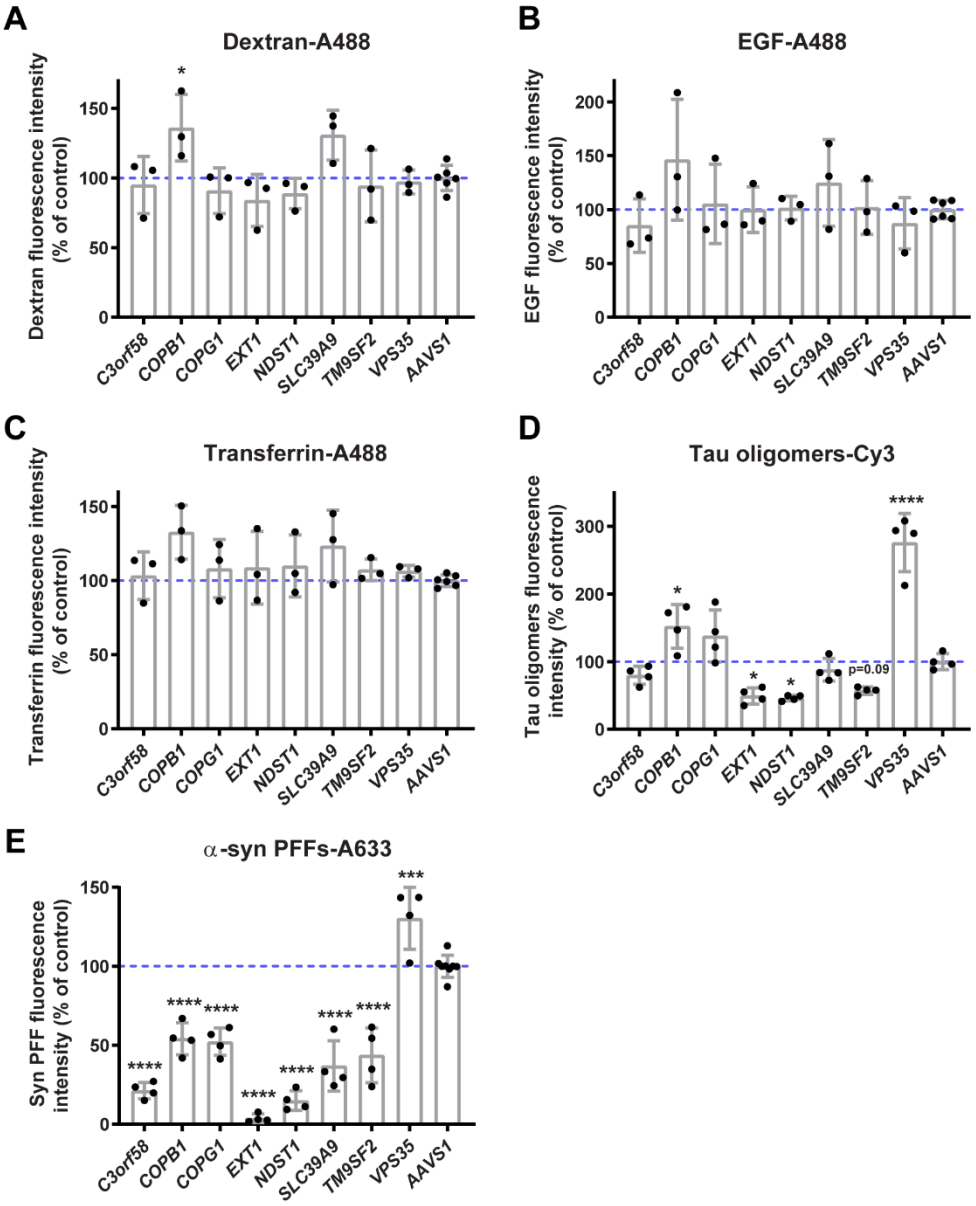

(A-E) RPE-1 cells stably expressing Cas9 nuclease were transfected in 96 wells plates with individual synthetic sgRNAs, and after 3 days, were subjected to 24 h uptake of the following cargoes: **(A)** dextran-Oregon Green 488, **(B)** EGF-A488, **(C)** transferrin-A488, **(D)** Tau oligomers-Cy3, and **(E)** α-syn-PFF-A633 as controls of sgRNAs' effects. Cells were then fixed, and nuclei stained with Hoechst 33342. Imaging was done using a CX7 high-content microscope and quantification with the HCS Studio Cell Analysis software. The mean total fluorescence intensity per cell was measured for each cargo. Images are shown in Suppl. Fig.4. Only Tau oligomers showed important changes in uptake upon invalidation of some hits, especially *EXT1*, *NDST1* and *TM9SF2* that are known to affect heparan sulfate expression, and *VPS35* which was previously reported to increase the uptake of proteinaceous aggregates. Intriguingly, *C3orf58* and *SLC39A9* did not significantly decrease Tau oligomers-uptake. Statistical test: one-way ANOVA: * $p<0.05$, *** $p<0.001$, **** $p<0.0001$.

Figure 4. – HSPGs are major receptors for α-syn PFF binding on the cell surface

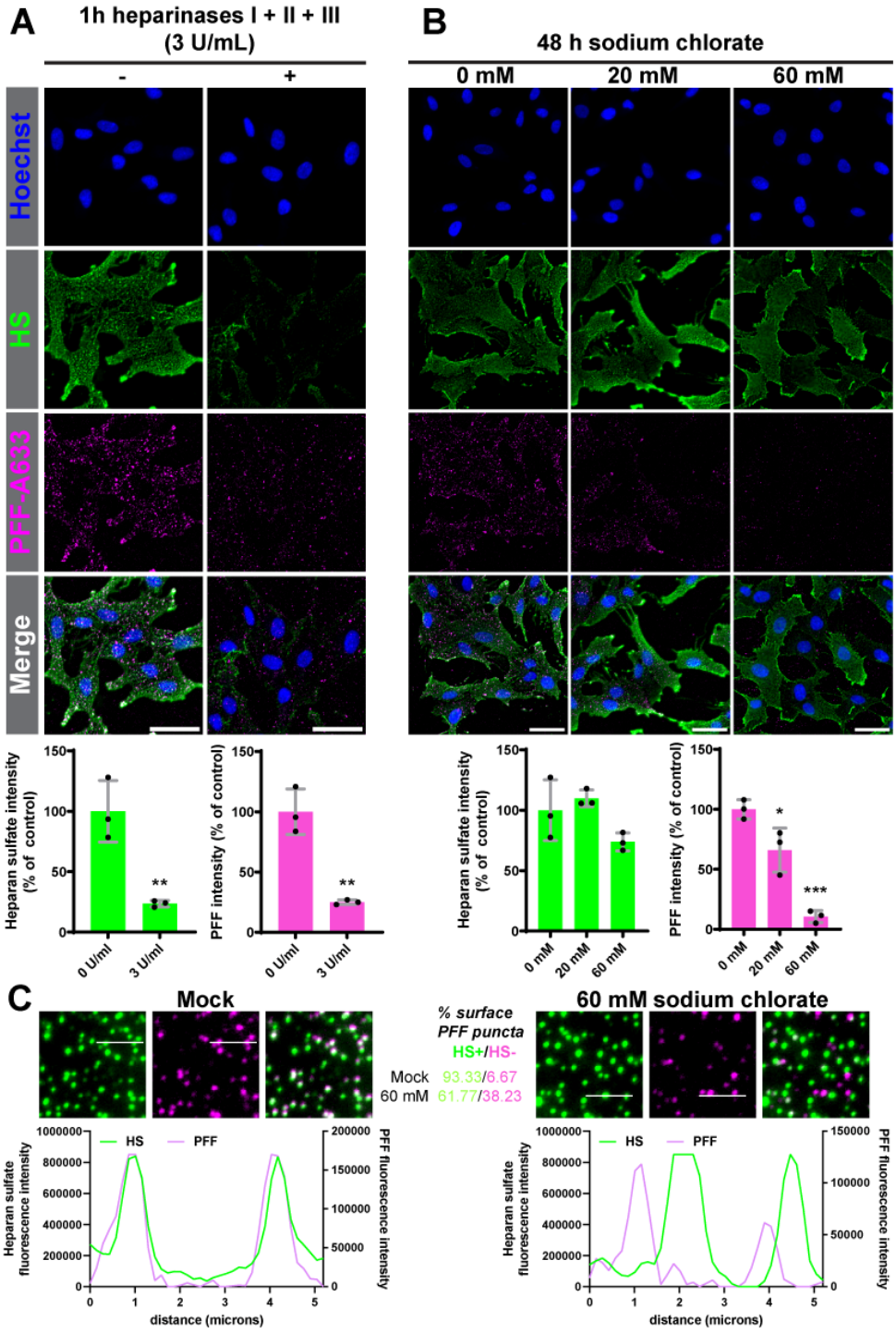

(A,B,C) PFF-A633 (magenta) binding and surface HS immunostaining (10e4 epitope, green) was performed on ice in live WT RPE-1 cells, before fixation and nuclei staining with Hoechst (blue). Before the binding assay, cells were pre-treated with a combination of heparinases I, II and III for 1h **(A)** or with sodium chlorate for 48h **(B,C)** at the indicated concentrations. Top panels show representative epifluorescence images at 20x **(A,B)** or 63x magnification **(C)**; bottom panels show quantifications performed with ImageJ. **(A,B)** Bar graphs are shown as mean ±SD percent of mock treated cells.

Statistical tests: **(A)** unpaired t-test or **(B)** one-way ANOVA; * $p<0.05$, ** $p<0.01$, *** $p<0.001$. Scale bars: 50 µm. **(C)** Cells from **(B)** were imaged at 63x, and the fluorescence intensity profiles along a 5.2 µm white line were measured and plotted for each set of images. Typical percentages of cell surface PFF puncta colocalized with an HS puncta (10e4 epitope), or not colocalized.

Figure 5. – Structure/function study of C3orf58 and SLC39A9

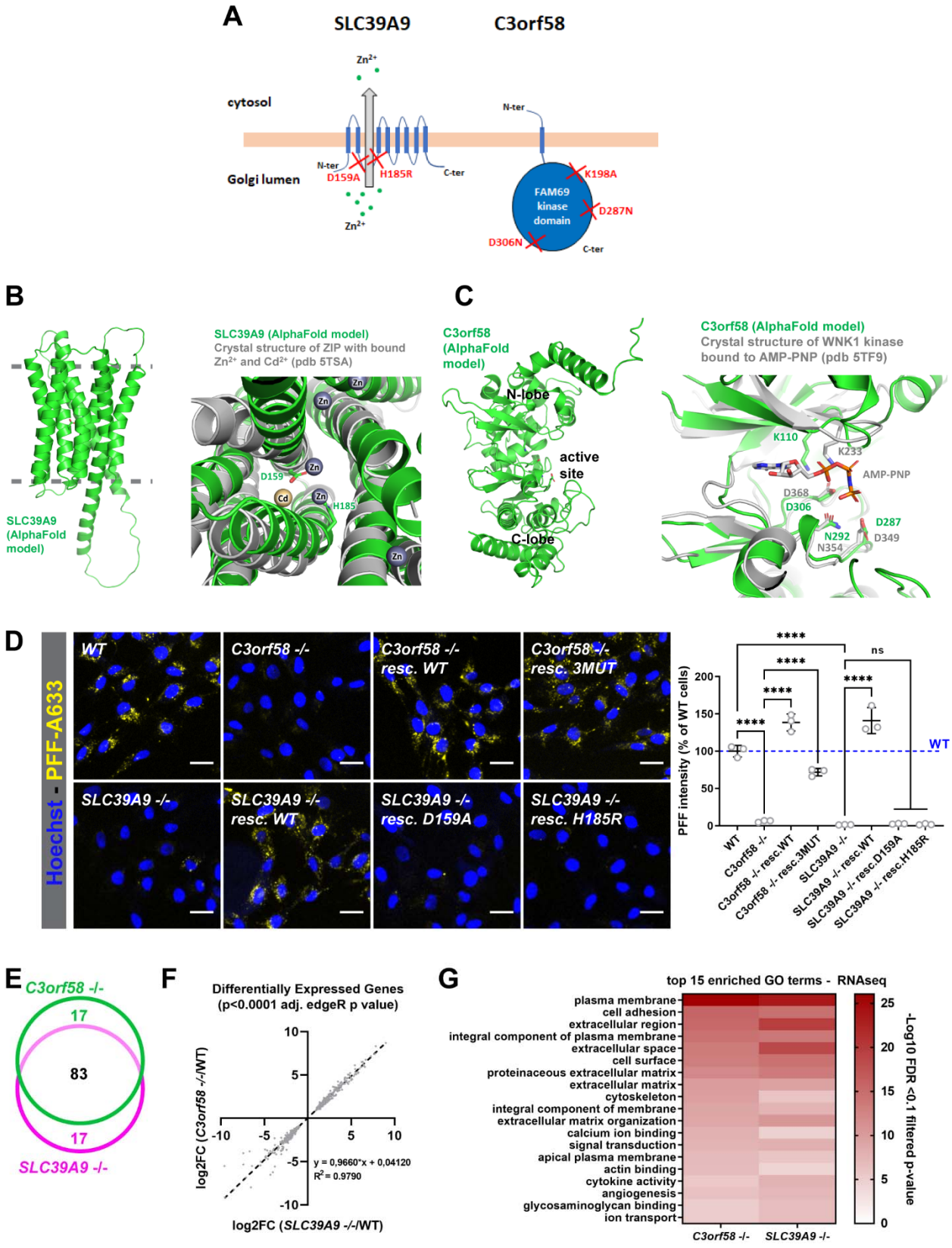

(A) Schematic representation of the topology of SLC39A9 and C3orf58 in the Golgi membrane. SLC39A9 is a Zn^{2+} transporter that exports Zn^{2+} from the Golgi lumen to the cytosol, whereas C3orf58 is a putative kinase of the FAM69 family. Designer mutations were engineered in both proteins (red crosses) to abolish the putative function of both proteins. For C3orf58, a triple mutant version of the protein was designed. **(B)** Left: global structure of SLC39A9, predicted by AlphaFold2 (AF-Q9NUM3-F1). The approximate position of the membrane bilayer is shown in grey. Right: structural superposition of SLC39A9 and the homologous zinc transporter ZIP bound to cadmium and zinc ions. Important residues for metal transport are shown as sticks. **(C)** Left: global structure of C3orf58, predicted by AlphaFold2 (AF-Q8NDZ4-F1). The protein harbors two lobes typically found in kinases, with a nucleotide-binding active site at the interface. Right: structural superposition of C3orf58 and the homologous kinase WNK1 bound to AMP-PNP. Important residues located around the active site are shown as sticks. **(D)** 24h uptake of 60 nM PFF-A633 (yellow) in *C3orf58* or *SLC39A9* monoclonal KO RPE-1 cells, either in absence or presence of stable expression of the indicated C-terminally HA-tagged rescue contructs. Nuclei were stained with Hoechst, and the mean PFF-A633 fluorescence intensity was quantified by high-content microscopy and normalized to WT RPE-1 cells (see graph, right panel). Statistical test: one-way ANOVA; ****p<0.0001. **(E-G)** RNA-seq analysis was performed to investigate transcriptomic changes in *SLC39A9* and *C3orf58* monoclonal KO cells at steady states, compared to WT RPE-1 cells. The edgeR package was used to perform differential expression and gene ontology analysis. **(E)** Venn diagram showing overlap between the top 100 differentially expressed genes in *C3orf58* KO and *SLC39A9* KO, compared to WT cells. **(F)** The magnitude of changes in gene expression were strikingly similar in both lines (R^2=0.9790 for genes with p<0.0001 common to both lines). **(G)** The top 15 GO terms of differentially expressed genes are shown. Of note, these 15 terms were identical between the two genotypes, indicating highly similar changes at the plasma membrane/cell surface in both KO lines.

Figure 6. PFFs binding to the cell surface is decreased in *C3orf58* and *SLC39A9* KO cells

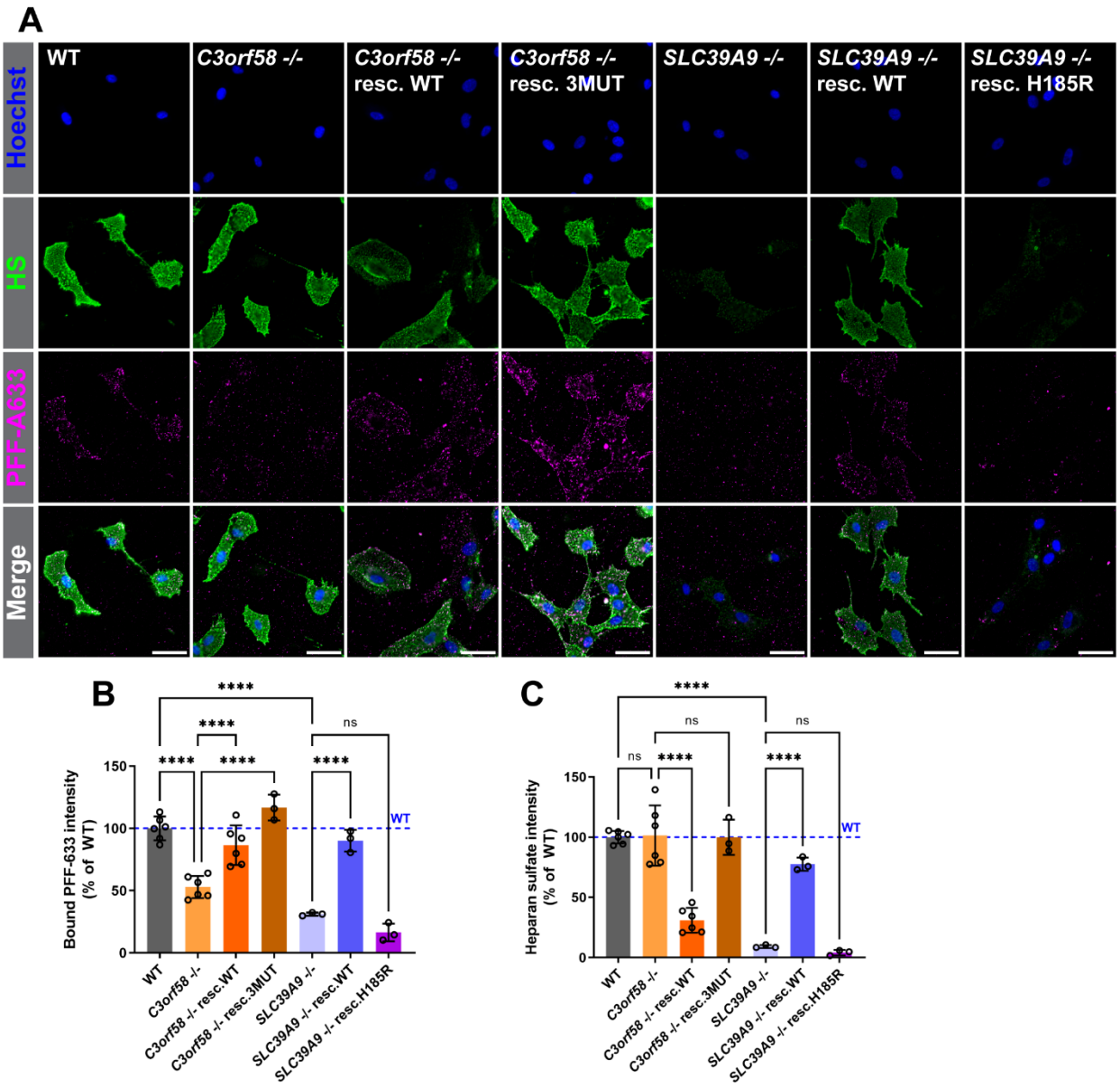

(A) PFF-A633 (magenta) binding and surface HS immunostaining (green) was performed on ice in live WT, *C3orf58* or *SLC39A9* monoclonal KO RPE-1 cells (± indicated rescue constructs), before fixation and nuclei staining with Hoechst (blue). Scale bar: 50 µm. **(B)** Mean HS (left panel) and PFF (right panel) signals per cell were quantified using ImageJ and are shown as percent of WT cells. Statistical test: one-way ANOVA; *** p<0.001, ****p<0.0001.

Figure 7. *C3orf58* and *SLC39A9* regulate HS levels and composition in RPE-1 cells

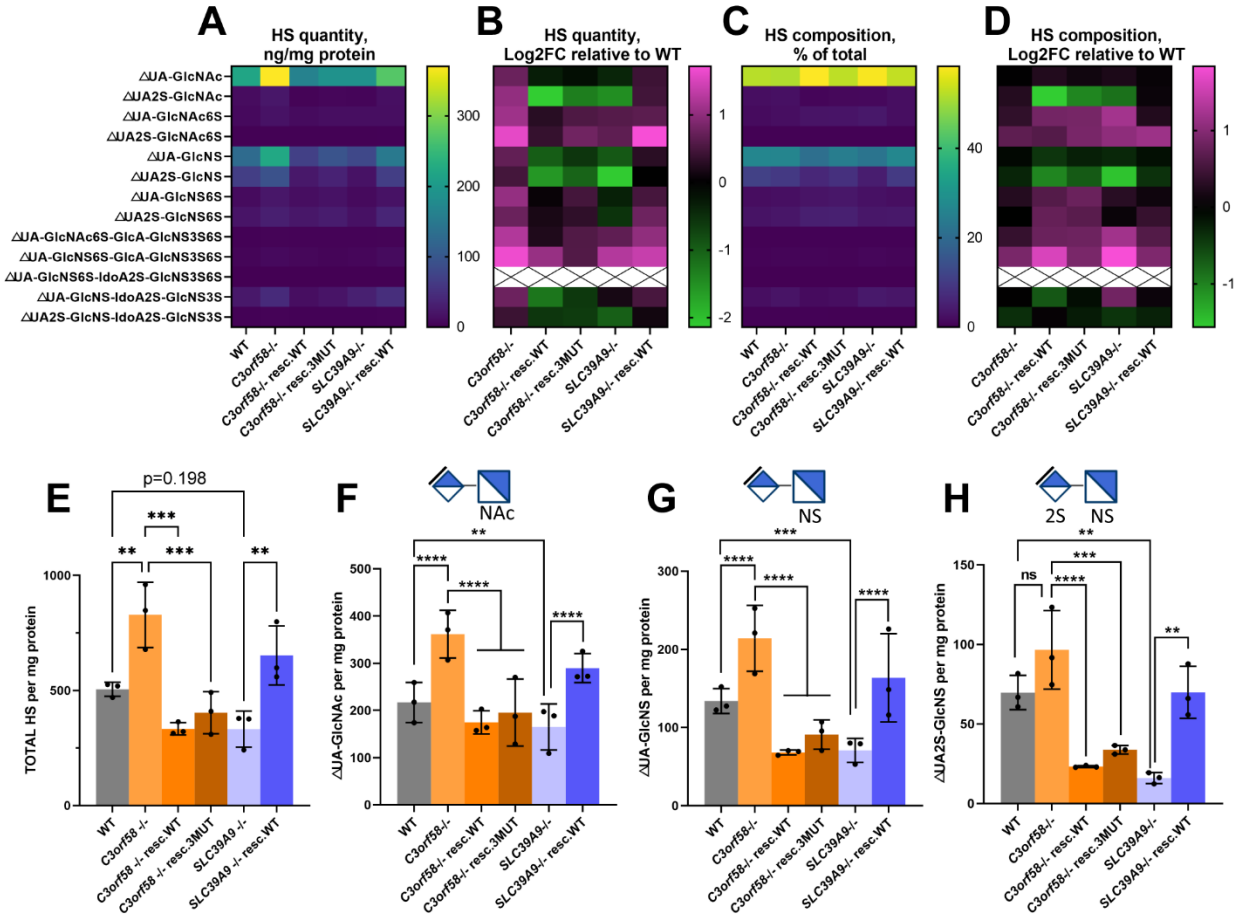

(A-G) Cell surface HS from WT, *C3orf58* or *SLC39A9* monoclonal KO RPE-1 cells (± indicated rescue constructs) were harvested by trypsin treatment before isolation and quantification of indicated HS disaccharides and tetrasaccharides by LC-MS/MS using ^{13}C-labeled internal standards. HS amounts were normalized to protein content from the cellular sample from which HS were isolated. **(A-D)** For each disaccharide/tetrasaccharide analyzed, we show as heat maps: **(A)** normalized quantities (ng/mg protein), **(B)** Log2 fold-change of normalized quantities relative to WT cells, **(C)** HS composition (percentage of each species relative to total HS), **(D)** HS composition as Log2 fold-change relative to WT. Black crosses on white background indicate an absence of detection in our samples. **(E-H)** Bar graphs showing normalized HS quantities of the indicated HS species: **(E)** total HS in samples, **(F)** ΔUA-GlcNAc, **(G)** ΔUA-GlcNS, **(H)** ΔUA2S-GlcNS. Statistical tests: one-way ANOVA; ** p<0.01, *** p<0.001, ****p<0.0001. See supplementary figure 16 for all disaccharide and tetrasaccharide quantification data.

Figure 8. *C3orf58* is important for PFF uptake in human microglia

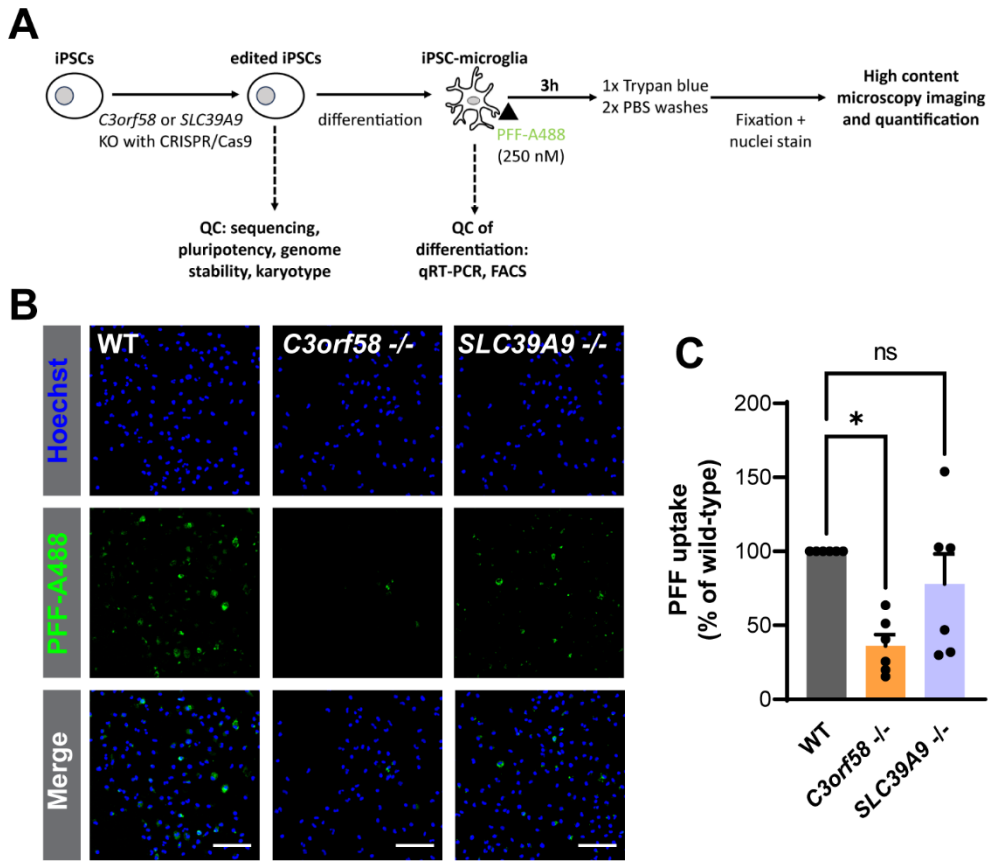

(A) Pipeline for generation of WT, *C3orf58* -/- and *SLC39A9* -/- iPSC-derived microglia (iMGL) used for performing α-syn PFFs uptake assay. Quality control of editing, genome stability and pluripotency is described in Supplementary Figure 18, and quality control of differentiation of the various lines in iMGL is shown is Supplementary Figure 19. **(B)** Representative images of α-syn PFFs uptake assay in iMGL of the indicated genotypes (scale bar: 250 µm), and **(C)** corresponding quantification showing a 60% reduction of α-syn PFFs uptake in *C3orf58* -/- iMGL compared to WT. Mean +/- SEM of n=6. Statistical test: Kruskal-Wallis; * $p<0.05$.